Supporting Information

Interplay between conformational dynamics and substrate binding regulates enzymatic activity: a single-molecule FRET study

David Scheerer*[a], Dorit Levy [a], Remi Casier [a], Inbal Riven [a], Hisham Mazal [a,b], Gilad Haran,*[a]

[a] Department of Chemical and Biological Physics, Weizmann Institute of Science, Rehovot 761001, Israel
[b] Max Planck Institute for the Science of Light, Erlangen 91058, Germany

Supporting Note 1: Model for substrate inhibition by AMP

Given that AMP inhibits AK's enzymatic activity and affects domain-closure dynamics, we postulated a correlation between these two phenomena (Scheme 1).[1] Our model is based on the hypothesis that different closed states can be sampled depending upon the order of ligand binding. Some of these states are incompatible with catalysis and must transition to a catalysis-prone state before the reaction occurs. Regardless of ligand binding, the enzyme can always exist in both open (blue) and closed (red) states. States are defined only for the ATP-binding LID domain. The rates for the interconversion between the states are defined for domain opening as k_o and for domain closing as k_c. Each substrate-bound species has specific opening and closing rates, designated by the superscript. The binding of AMP to the NMP domain is unaffected by the LID domain's status, allowing both open and closed states to bind AMP. However, ATP can bind only to the open state.

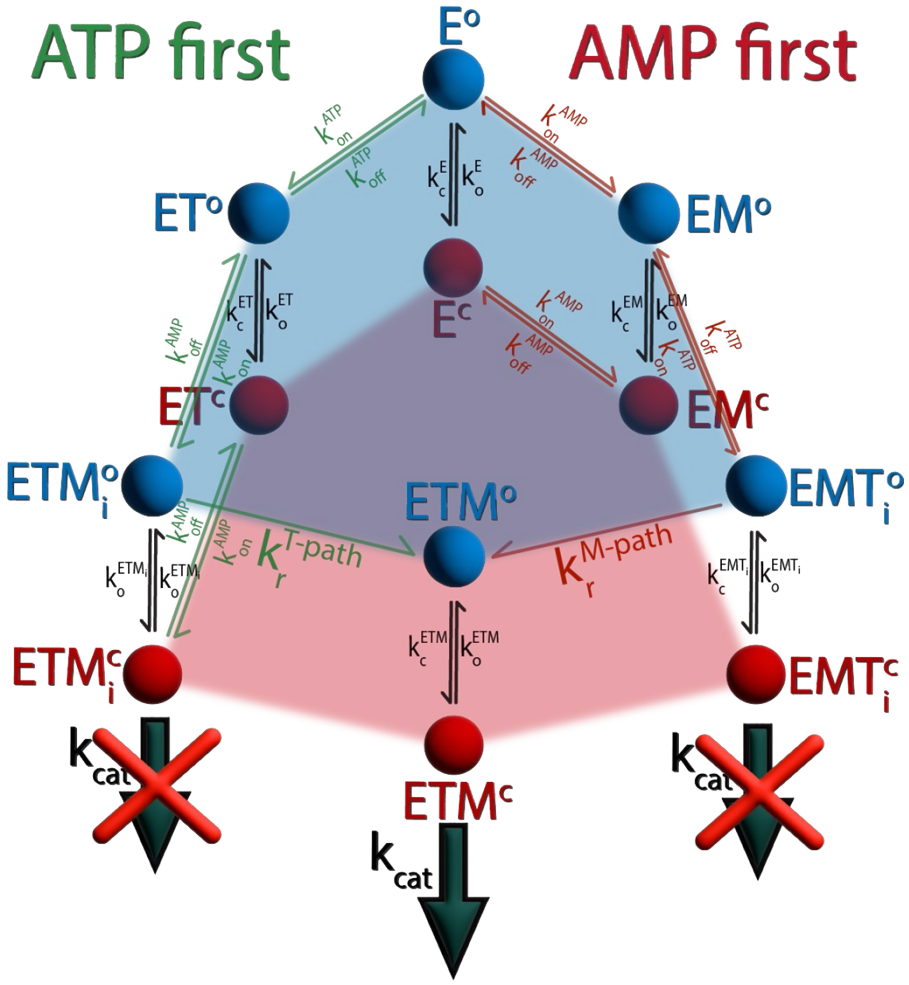

Scheme 1. Mechanism for the substrate inhibition in AK, based on two competing pathways.

The model in Scheme 1 leads to two scenarios regarding the order of nucleotide binding to the apoenzyme E. ATP can only bind if the LID domain is in the open state (E^o). Should ATP bind first, this results in the ATP-bound state ET. Both the open (ET^o) and closed conformation (ET^c) of ET can subsequently bind AMP, forming the double substrate-bound state ETM_i. The initial encounter complex ETM_i can exhibit diverse substrate binding poses, often

differing significantly from the native structure.[2] Catalysis is contingent upon the substrates repositioning themselves into the correct pose, denoted as ETM^o, a process governed by the rearrangement rate constant k_r^{T-path}. Conversely, if AMP binds first at the NMP domain, it yields the EM^o and EM^c complexes. The consequent binding of ATP leads to the formation of EMT_i. Similar to ETM_i, we postulated that the substrates in this complex require rearrangement (with the rate constant k_r^{M-path}) to achieve the productive ETM state. ETM_i and EMT_i are distinguished by their binding order —ATP first, then AMP or vice versa— based on the hypothesis that initial AMP binding may result in a limited or different sampling of the nucleotide orientation.[3] One reason might be that AMP binds in an orientation closer to the native binding pose when ATP is already bound and the LID domain is preferentially closed. A small rate constant k_r^{M-path} effectively imposes a kinetic barrier within the "AMP first" path. The conversion of the inactive ETM_i and EMT_i states to the productive ETM state only occurs through their open states, as suggested recently by our molecular dynamics simulations.[2] The rates of phosphotransfer in the ETM state and subsequent product dissociation are combined in k_{cat}. The rate constants for binding AMP or ATP are defined as k_{on}^{AMP} and k_{on}^{ATP}, respectively. Instead of being converted to ADP, the substrates can also dissociate with the rates k_{off}^{AMP} and k_{off}^{ATP}.

Essentially, the model introduces a kinetic barrier for the path in which AMP binds first. In a typical AK activity assay conducted under saturating ATP concentrations, the flux through the "ATP first" pathway predominates over that of the "AMP first" pathway at low levels of AMP (Fig. S20). However, as AMP levels rise, a larger fraction of the total flux diverts towards the "AMP first" path involving the unproductive ETM_i state, consequently diminishing the enzymatic velocity. Urea has the potential to influence both the conformational equilibrium and the affinity for AMP, thereby altering the flux in either of the two pathways.

Supporting Note 2: Analysis of binding-state-dependent opening and closing rates

The occupancy of the closed state in AK is dependent on the substrate concentration. Each substrate-bound species is presumed to have specific opening and closing rates. Our focus was primarily on the effect of AMP on the protein dynamics of the ATP-bound species. It was observed that minor AMP concentrations (<500 µM for the WT without urea) did not result in significant alterations in the opening and closing rates (Scheme 2a).

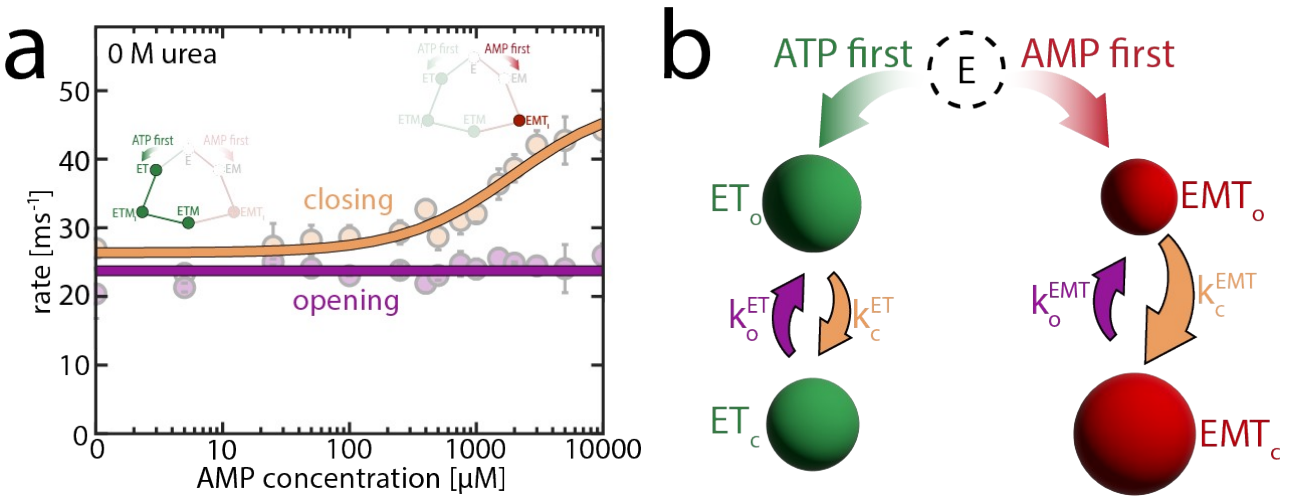

Scheme 2. Binding-state dependent opening and closing rates.

In this concentration range, the "ATP first" path is predominantly populated. Given the high enzymatic velocity at ~400 µM AMP (Fig. 1a main text), both the ETM_i and ETM state are likely populated to some extent. The absence of significant impact on the protein dynamics suggests that our single-molecule experiments cannot distinguish between the ET and the ETM/ETM_i species under these conditions. In Scheme 2b, these species are referred to as ET. In contrast, inhibitory concentrations of AMP above 500 µM increase the apparent closing rate (orange line in Scheme 2a), which we attribute to an increasing population of the "AMP first" pathway, particularly the inactive EMT_i state (denoted as EMT in Scheme 2b). In this scheme, we consider the enzyme as always bound to ATP, given that [ATP] » K_d(ATP). The different open enzyme species contribute to the apparent closing rate k_c^{app} in proportion to their populations. The concentration of the more productive species ET/ETM/ETM_i is denoted as $[ET]$, while the concentration of molecules in the inactive EMT_i species is denoted as $[EMT]$, giving

$$k_c^{app} = \frac{[ET]}{[ET]+[EMT]} \cdot k_c^{ET} + \frac{[EMT]}{[ET]+[EMT]} \cdot k_c^{EMT} = \frac{c_{50,AMP} \cdot k_c^{ET} + [M] \cdot k_c^{EMT}}{c_{50,\ AMP} + [M]}, \quad (1)$$

with $[M]$ as the AMP concentration, k_c^{EMT} as the closing rate of EMT_i species, k_c^{ET} as the closing rate of ET/ETM/ETM_i. $c_{50,AMP}$ is the AMP concentration at which both the ET and EMT species are equally populated.

$$c_{50,AMP} = \frac{[ET] \cdot [M]}{[EMT]} \quad (2)$$

Without urea, AMP does not significantly affect the apparent domain opening rate, so it was treated as constant over the complete AMP range (violet line in Scheme 2a). In contrast, an increase in the opening rate was detected with

0.8 M urea present (Fig. 4 main text). In this case, the opening and closing rates were globally optimized according to Eq. (1) and (3).

$$k_c^{app} = \frac{[ET]}{[ET]+[EMT]} \cdot k_o^{ET} + \frac{[EMT]}{[ET]+[EMT]} \cdot k_o^{EMT} = \frac{c_{50,AMP} \cdot k_o^{ET} + [M] \cdot k_o^{EMT}}{c_{50,\ AMP} + [M]}, \quad (3)$$

with k_o^{EMT} as the opening rate of EMT_i species and k_o^{ET} as the opening rate of ET/ETM/ETM_i.

In the absence of ATP, the effect of AMP on protein dynamics is weak.[1] Opening and closing rates for the EM species were measured in the presence of 5 mM AMP.

Supporting Methods

Protein Expression and Labeling. E. coli AK C77S gene with a six-residue histidine tag at its N-terminus was cloned in pET15b vector. All AK mutants were generated by site-directed mutagenesis and standard cloning techniques in pET15b and were verified by DNA sequencing. AK mutants were transformed into E. Coli BL21 (DE3) pLysS cells (Invitrogen) using heat shock and grown in the presence of Ampicillin up to OD 0.6–0.8 at 37 °C. Protein expression was induced by adding 1 mM IPTG and cells were then incubated at 25 °C overnight. Following expression, bacteria were harvested, and proteins were purified using FF crude HisTrap column (GE Healthcare) with an elution step involving 250 mM imidazole. Imidazole was then removed by overnight dialysis and the protein was kept with 50% glycerol at -20 °C until used. Labeling reactions were performed by first incubating protein samples with Alexa 594 maleimide (Invitrogen) at a 1:0.8 protein to dye molar ratio for 2 h at 25 °C, followed by incubation Alexa 488 maleimide (Invitrogen) at a 1:2 protein to dye molar ratio for additional 2 h at 25 °C. Finally, labeled proteins were separated from the unreacted dye using HiTrap desalting column (GE Healthcare).

smFRET measurements

Single-molecule data was acquired on freely diffusing molecules using a Microtime 200 system (PicoQuant). Flow cells were prepared as described previously[4] and filled with a mixture of 30 pM labeled enzyme, 50 mM Tris-HCl (pH 8.0), 100 mM KCl, 5 mM $MgCl_2$, 0.01% Tween (Thermo Fisher), and substrates (ATP, ADP, AMP; Sigma). Importantly, we used ^{31}P-NMR spectroscopy to verify that our ATP solutions contained no ADP. Substrate concentrations used for experiments under turnover conditions are given in Table S4. The appropriate ADP concentration to guarantee equilibrium (zero flux) was calculated using the following rate equation:

$$v \propto \frac{k_1[M][T]}{K_{D,T}K_{D,M}} - \frac{k_{-1}[D_1][D_2]}{K_{d,D1}K_{d,D2}}, \tag{4}$$

where k_1/ k_{-1} are the forward and backward rate constants for the reaction and [M] and [T] are the AMP and ATP concentrations. $K_{d,S}$ is defined as the dissociation constant of the respective substrate (T,M,D_1,D_2) and values were taken from Sheng *et al.*.[5] [D_1] and [D_2] are the concentrations of ATP bound to the LID and NMP domain, respectively. [D_2] was calculated using

$$[D_2] = \frac{\frac{1}{K_{Mg}} + [D] + [Mg] - \sqrt{\left(\frac{1}{K_{Mg}} + [D] + [Mg]\right)^2 - 4 \cdot [D] \cdot [Mg]}}{2}, \tag{5}$$

where [Mg] and K_{Mg}[5, 6] are the concentration and dissociation constant for magnesium, respectively. FRET efficiency histograms from the first and last 1 h of each measurement were shown to overlap, validating that the substrate concentration did not change during the measurement.

Recoloring analysis

We performed a recoloring analysis to verify the parameters obtained from the H^{2}MM analysis.[4, 7] In this method, the arrival times of photons in each data set are retained, but their "colors" (i.e. whether they belong to the donor or acceptor) are erased. A stochastic simulation based on the H^{2}MM parameters is then used to reassign the photons to the two experimental channels, and FRET efficiency histograms are reconstructed. A good match between the original and recolored histograms indicated a successful analysis.

Dwell-time analysis

The dwell-time analysis yielded the distributions of times the protein spends in each state (in this case, the open and closed state). Here, we computed these distributions using a likelihood-weighted segmentation algorithm developed in-house.[8, 9] In this analysis, for each burst, every possible sequence of states contributes a fraction of a count to each dwell time, equal to the likelihood of the sequence. In contrast with the more common dwell-time analysis based on the Viterbi algorithm, all possible state sequences were considered, not only the most likely one. A good agreement of rates obtained directly from the H^{2}MM analysis and those obtained from the dwell-time analysis was taken as a validation of the analysis (Table S3).

Time-resolved burst variance analysis (trBVA)

To further validate the presence of dynamics on a µs-time scale, we employed trBVA, a recently published time-resolved version of burst variance analysis that can quantify kinetic rates at microsecond to millisecond timescales.[10] Bursts were partitioned into segments with a fixed number of photons. The FRET variance was computed from these segments and compared with the variance expected from shot noise. Systematically varying the segment size can capture dynamics at different timescales. For this analysis, we utilized the same bursts as for H^{2}MM. To minimize the impact of photophysical artifacts, we removed windows where consecutive photons of the same color are more than 30 µs apart. This allowed us to fit the data to a two-state model.[10]

Time-resolved fluorescence anisotropy

To validate that urea did not have unwanted side effects on dye mobility, we measured fluorescence anisotropy decays of the dyes in the presence of urea. Single-labeled AK molecules were diluted to ~ 1-2 nM, loaded into a flow cell and measured in a MicroTime200 microscope as described in the main text, but with the following modifications. Molecules were excited with a polarized laser at either 495 nm or 594 nm. The emitted photons passed through a polarizing beam splitter cube, which split the photons according to their polarization into parallel and perpendicular channels. The split photons passed through emission filters for the donor and acceptor labeled samples, and their arrival times relative to the laser pulse were recorded. The fluorescence anisotropy decay curve for each sample was calculated using the following equation:

$$R(t) = \frac{I_{\parallel}(t) - I_{\perp}(t)}{I_{\parallel}(t) + 2I_{\perp}(t)}, \tag{6}$$

where $I_{\parallel}(t)$ and $I_{\perp}(t)$ are the temporal intensities of the parallel and perpendicular components, respectively, relative to the laser pulse.

Preparation of urea solutions

Solutions for measurements in the presence of urea were prepared immediately before the experiment. The urea concentration was determined by measuring its index of refraction using a Fisher-Abbe refractometer (Fisher Scientific Co.), according to the equation below:[11]

$$[urea] = 117.66 \cdot \Delta n + 29.753 \cdot \Delta n^2 + 185.56 \cdot \Delta n^3, \quad (7)$$

where $[urea]$ is the concentration of urea, and Δn is the difference between the index of refraction of buffer with and without urea. Due to the high ionic strength, the pH of the urea solutions had to be corrected by using the equation below:[12]

$$pH_{real} = pH_{app}\left(- 0.394 \cdot [urea] + 0.06015 \cdot [urea]^2 - 7.157 \cdot 10^{-3} \cdot [urea]^3 + 3.382 \cdot \right), \quad (8)$$

where pH_{real} is the corrected pH and pH_{app} the apparent pH measured by the pH-meter.

Circular dichroism spectroscopy

The unfolding status of the protein was monitored by the circular dichroism (CD) signal at 222 nm (Fig. S4). In the concentration range used for the enzymatic essays and smFRET experiments (0-0.8 M urea), the secondary structure content of AK does not change. The solid lines in the figure indicate fits to a sigmoidal function with flat baselines:[13, 14]

$$\theta_{222nm} = \frac{\theta_N + \theta_U \cdot K_{obs}}{1 + K_{obs}}, \quad (9)$$

where θ_N and θ_U is the molar ellipticity of the native and unfolded state, respectively. K_{obs} is given by:

$$K_{obs} = \exp\left(\frac{-\Delta G^0_{fold} - m * [urea]}{R * T}\right), \quad (10)$$

with ΔG^0_{fold} the folding free energy difference without urea, the m-value being the proportionality constant for the effect of urea concentration, R the gas constant and T the absolute temperature.

Microscale thermophoresis

The affinity values of AMP and ATP to AK were measured using the microscale thermophoresis (MST) instrument Monolith NT.115 (Nano-Temper Technologies). A series of 10 µL solutions at different substrate concentrations was prepared. Each solution was mixed with a 10 µL solution containing AK molecules labeled with Alexa488 to obtain a final AK concentration of 30 nM and loaded into a special coated capillary supplied by Nano-Temper. Fluorescent molecules were excited with a blue laser (470 nm, 50% LED power) to monitor the spatial distribution of molecules in the capillary. Thermophoresis was measured in each capillary by locally heating a defined sample volume with a focused infrared laser (40% MST power) for 30 s. Protein molecules diffused away from the peak of the temperature gradient formed by the laser. Bound and unbound molecules responded differently, which led to a different steady-state spatial distribution of fluorescence. The change in depletion in the presence of substrate was plotted and used to calculate the bound protein fraction. The dissociation constant was then obtained by fitting the results to a binding isotherm.

Fitting enzymatic activity

To fit enzymatic velocity based on the kinetic model described in Supporting Note 1: "Model for the substrate inhibition by AMP", we used experimentally observed opening and closing rates of the LID domain for the different substrate-bound species as inputs. These rates were determined as described in Supporting Note 2: "Analysis of binding-state dependent opening and closing rates" and are listed in Table S5. The protein dynamics of the ET, ETM_i and ETM species were assumed to be the same, as minor concentrations of AMP (< 1000 μM) did not affect the opening and closing rates (Fig. 4, main text). The open and closed states are defined only for the ATP-binding LID domain. It was assumed that ATP can bind only to the open state, while AMP can bind to both open and closed states, as it binds to the NMP domain.

For the WT, experimental substrate affinities were provided as an input. The dissociation constants of AMP, K_d (AMP), and ATP, K_d (ATP), as a function of urea concentration were determined by MST, as discussed in the previous section. K_d (AMP) increased 2.3-fold by urea (Fig. 2 main text), while K_d (ATP) was only slightly increased by urea, in agreement with the results of Rogne *et al*.[13] Explicit substrate binding and dissociation rates were treated as free parameters, but were required to maintain the experimental K_d values; AMP can bind to both the LID-open and -closed state; accordingly, K_d (AMP) is given by

$$K_d(AMP) = \frac{k_{off}(AMP)}{k_{on}(AMP)}, \tag{11}$$

with k_{on} (AMP) the binding rate constant for AMP and k_{off} (AMP) the dissociation rate. As ATP can bind and unbind only in the open state, we took into account the conformational equilibrium in the bound ($K_{C,ET}$) and unbound ($K_{C,E}$) species for the dissociation constant of ATP,

$$K_d(ATP) = \frac{k_{off}(ATP)\cdot\left(K_{C,E}+1\right)}{k_{on}(ATP)\cdot\left(K_{C,ET}+1\right)}, \tag{12}$$

with k_{on} (ATP) as the binding rate constant for ATP and k_{off} (ATP) as the dissociation rate. Lower limit for substrate dissociation rates of k_{off} (ATP) ≥ 544 s^{-1} and k_{off} (AMP) ≥ 6340 s^{-1}, provided by Fry and coworkers,[15, 16] were used in the fitting procedure.

Other free parameters were the rate of the actual phosphotransfer step (k_{cat}) and the rate of the correct positioning of substrates in the "ATP first" path k_r^{T-path} and the "AMP first" path k_r^{M-path}. These parameters were considered as unaffected by urea. While it is possible that urea also affects k_r and k_{cat}, the impact is likely minimal as enzymatic velocity is accurately described with these parameters shared across different urea concentrations. All free parameters were optimized globally to match the enzymatic turnover as a function of either AMP or ATP concentration. In this procedure, we formulated a set of differential equations that describe the kinetics in Supporting Note 1. The concentration of any involved species was calculated by integrating these differential equations, which was done numerically using MATLAB's ordinary differential equation solver ode15s.[17] The change of the substrate

concentration over time represents the turnover v_0. This calculation was repeated for different initial concentrations of urea and the substrates. Finally, we used a χ^2-minimization of v_0 versus the substrate concentration to optimize the free parameters. The goodness of the fit in each case was judged based on the reduced χ^2 values.

As expected, the optimized parameters for binding rate constants of k_{on} (ATP) = $1.9 \cdot 10^7$ M^{-1} s^{-1} and k_{on} (AMP) = $8.6 \cdot 10^7$ M^{-1} s^{-1} are 1-2 orders of magnitude smaller than the diffusion limit, which was evaluated from the well-known Smoluchowski equation,

$$k_{D_0} = 4\pi DR, \tag{13}$$

where D is the relative translational diffusion constant and R is the contact distance between the centers of the two molecules.

In the case of the mutant proteins L107I and F86W, the binding rate constants of the WT were provided as inputs, assuming that the encounter rate between substrate and enzyme is unaffected by the mutations. The dissociation rates were treated as free parameters, as the mutations likely affect the interactions between the protein and the bound substrate, in particular for F86W with the mutation in the AMP binding site.[18] This means that for the mutant proteins the K_d values were not constrained. For F86W, which does not show substrate inhibition, a simplified model containing only the "ATP first" path was used. Our single-molecule experiments did not detect statistically significant differences ($P > 0.05$, Student's t-test) in the protein dynamics between E and EM, as well as between ET and EMT_i, suggesting that the "AMP first" path is only weakly populated. It is plausible that the mutation of F86 prevents the formation of the inactive EMT_i orientation of the nucleotides.

To estimate the confidence intervals of the fitted parameters, we monitored the increase in χ^2_{red} (χ^2 per degree of freedom) upon the perturbation of each parameter. For this, we used the optimized values from the χ^2-minimization (Table 1, main text) and fixed the tested parameter at different values surrounding the optimal one. Then, the remaining parameters were optimized under this constraint. Afterwards, we calculated the difference in χ^2_{red} with and without the constraint. A sharp increase in $\Delta\chi^2_{red}$ indicates that the goodness-of-fit is highly sensitive to the tested parameter. To distinguish between urea's effect on conformational dynamics and substrate affinity, we tested computationally how the enzymatic velocity would change when only one of the parameters is affected by urea at a concentration of 0.8 M while preserving all other parameters as determined at 0 M urea. Finally, to evaluate how enzymatic velocity depends on the actual opening and closing rates, we scaled the experimentally derived closing and opening rates of the ATP-bound species (ET, ETM_i, EMT_i, ETM) by a factor between 0.01 and 100. The conformational dynamics of species that are not bound to ATP (E, EM) were not altered as they are hardly affected by urea (Fig. 3c, main text).

Supporting Figures

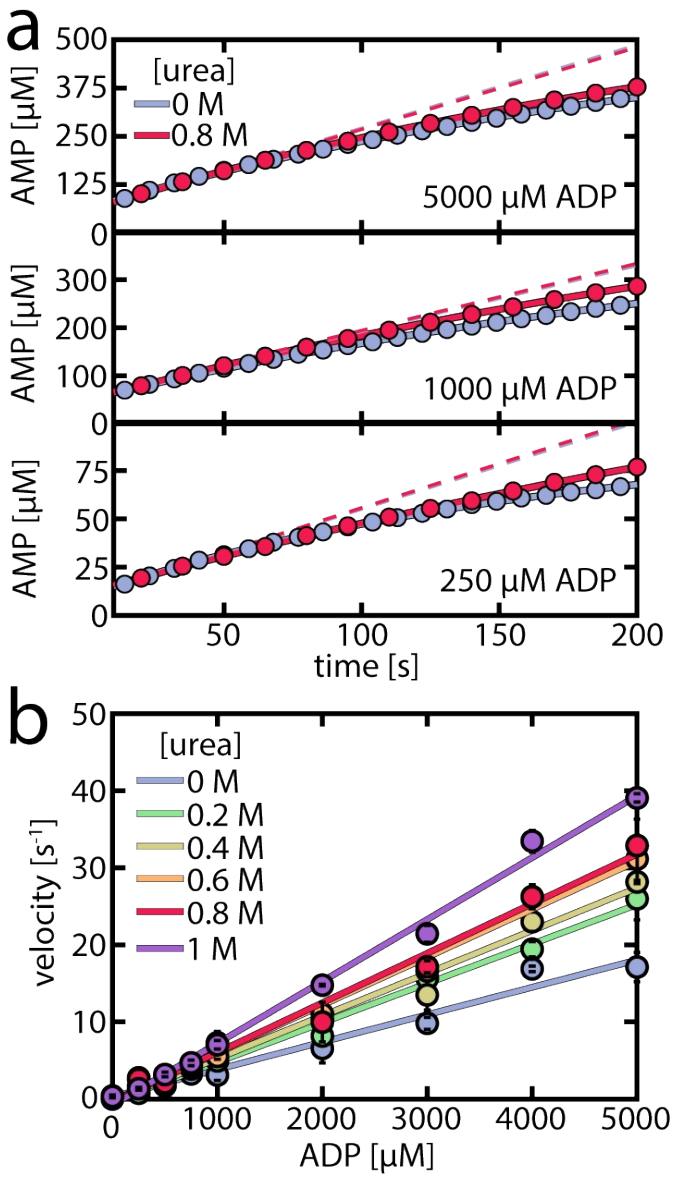

Figure S1: Effect of urea on the AMP inhibition of the backward reaction. a) Shown is the AMP concentration following the start of the reaction by injection of Mg^{2+} for representative initial ADP concentrations of 5000 µM (top), 1000 µM (center) and 250 µM (bottom) and for urea concentrations of 0 M (blue) and 0.8 M (red). The curves at 0.8 M urea represent the data shown in Fig. 1d in the main text. The solid curves represent a fit according to Eq. (1) (main text). The dashed lines represent the extrapolated product formation without product inhibition. While the initial velocities v_0 are not significantly affected by urea (Fig. 1d, main text), product inhibition by AMP is weaker in the presence of urea. b) Enzymatic velocity of WT AK as a function of ADP concentration in the presence of 10 mM AMP. For the backward reaction, AMP is a competitive inhibitor for the ADP/AMP binding site, resulting in a strong reduction of turnover and an apparent linear dependence on the ADP concentration. Urea (blue to violet curves) gradually alleviates the inhibition by AMP. Error bars indicate the standard error of the mean of 3 measurements.

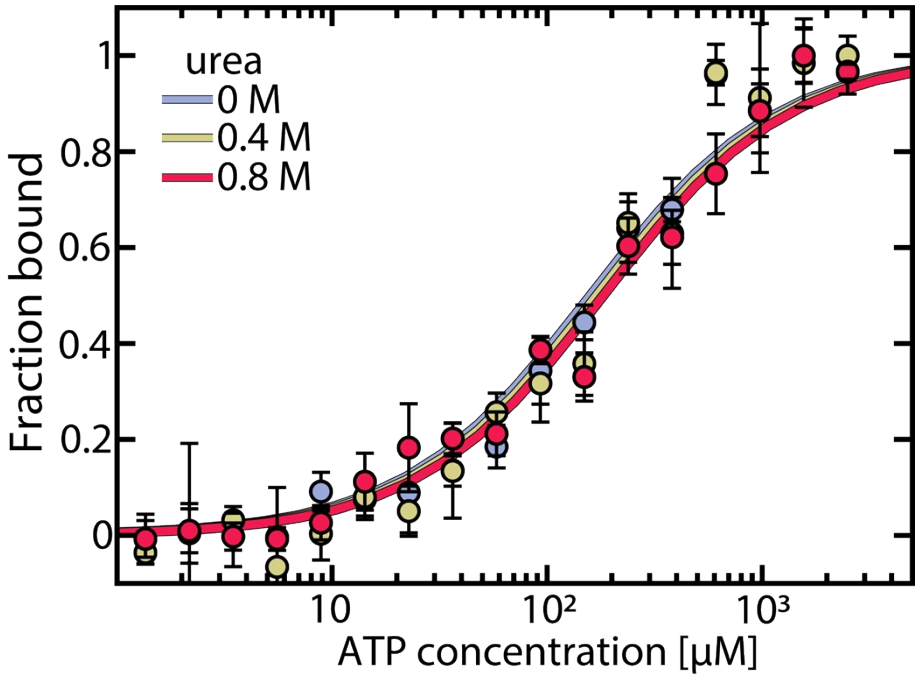

Figure S2: ATP binding to AK measured by MST. The fraction of bound AK as a function of ATP concentration was measured at urea concentrations of 0 M (blue), 0.4 M (yellow) and 0.8 M (red). Data was fitted to obtain K_d (ATP) values of 159 ± 17 µM, 170 ± 23 µM and 183 ± 18 µM, respectively. Error bars indicate the standard errors of the mean of 3 measurements.

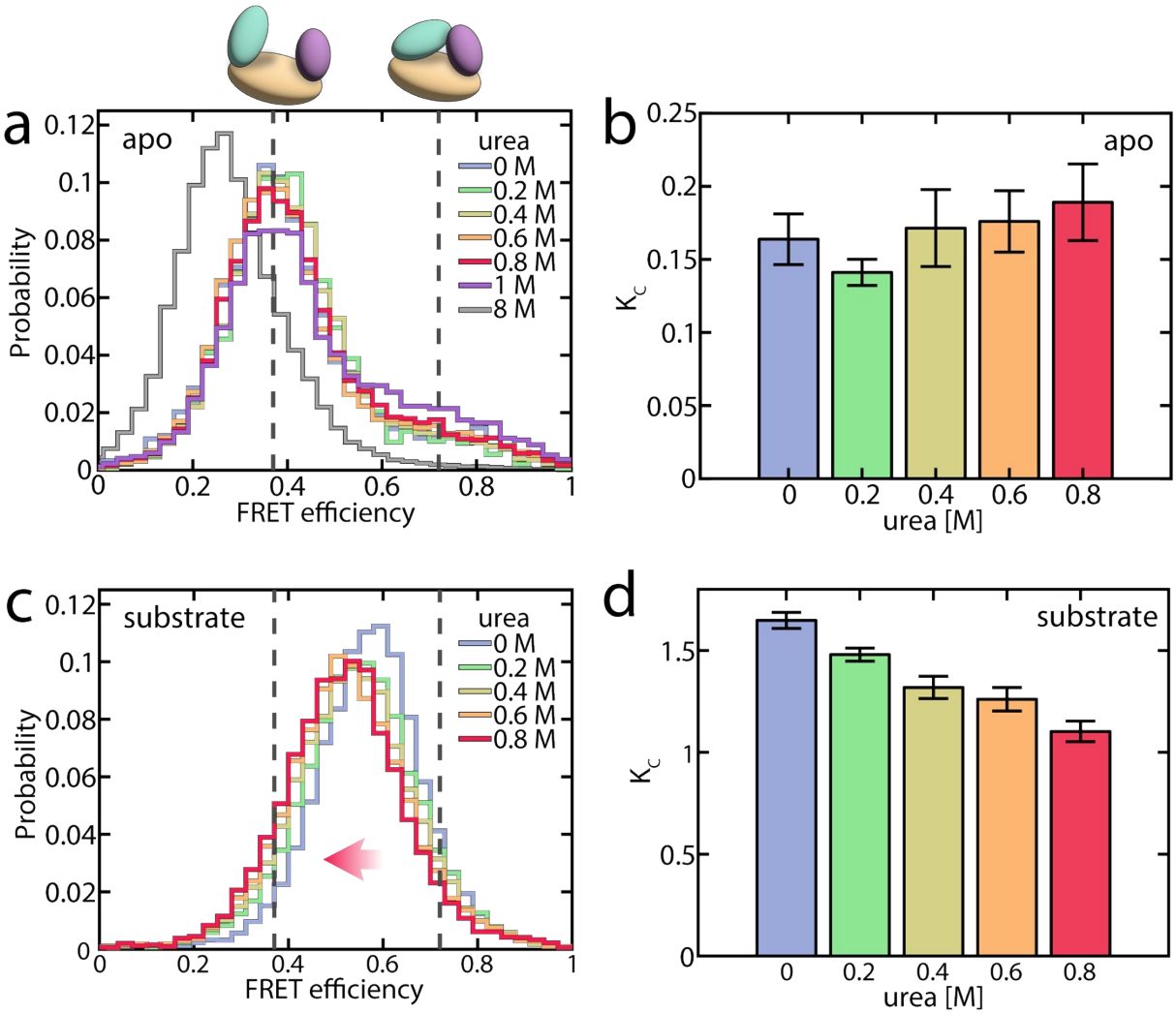

Figure S3: Effect of urea on AK's conformation without and with substrate. a) FRET efficiency histograms of the apoprotein at a series of urea concentrations. The dashed grey lines indicate the FRET efficiency values of the open (0.37±0.01) and closed (0.72±0.01) states obtained from the H^{2}MM analysis. The impact of urea on the FRET efficiency histogram was minimal at concentrations up to 0.8 M. However, at 1 M urea (violet), a notable shift toward higher FRET efficiencies was observed. This behavior contrasts with the low-FRET efficiency state associated with the fully unfolded protein at 8 M urea (grey). The shift at 1 M urea likely reflects the presence of a small fraction of molecules occupying a more compact folding intermediate with an unfolded LID domain.[19, 20] b) Change in the equilibrium coefficient K_C ratio as determined by H^{2}MM for the apoprotein. c) In the presence of 1 mM ATP, 5 mM AMP and 417 µM ADP, increasing urea concentrations shift the histogram towards lower FRET efficiencies. d). As in (b), in the presence of substrates. Error bars indicate the standard error of the mean of at least 3 repeated measurements.

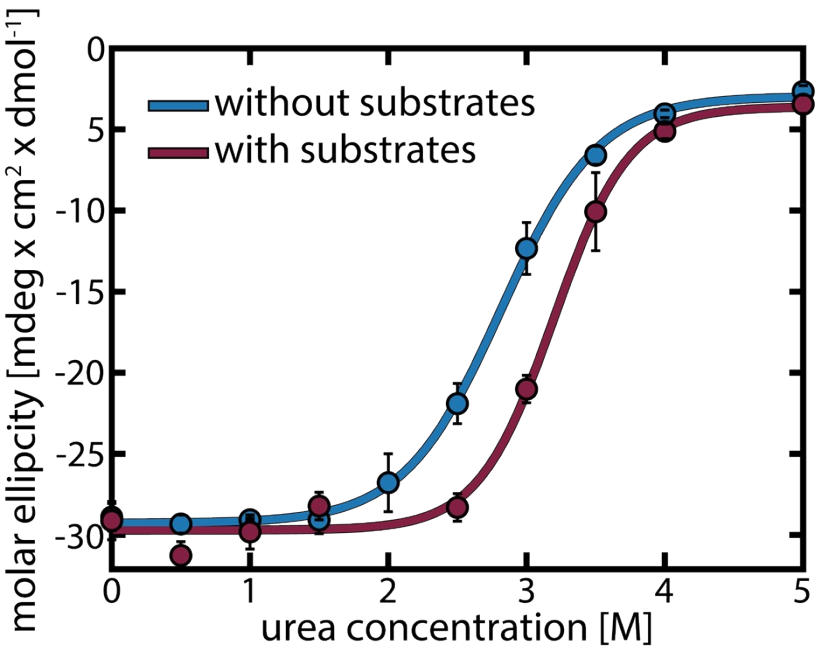

Figure S4: Stability against urea-induced unfolding. a) The unfolding of secondary structure elements in AK (AK C77S/V142C/A73C) was monitored by the CD signal at 222 nm in the absence (blue) or presence (red) of substrates. In the concentration range used for the enzymatic essays and smFRET experiments (0-0.8 M urea), the α-helical content of AK does not change, similarly as for the WT protein.[21, 22] The solid lines indicate fits to a sigmoidal function with flat baselines (Eq. (8)). The resulting values for the Gibbs free energy of folding, ΔG^{0}_{fold}, the m-value for denaturant-dependent unfolding and the midpoint of the transition are given in Table S6. The binding of substrates increased the stability of AK, as observed before.[19]

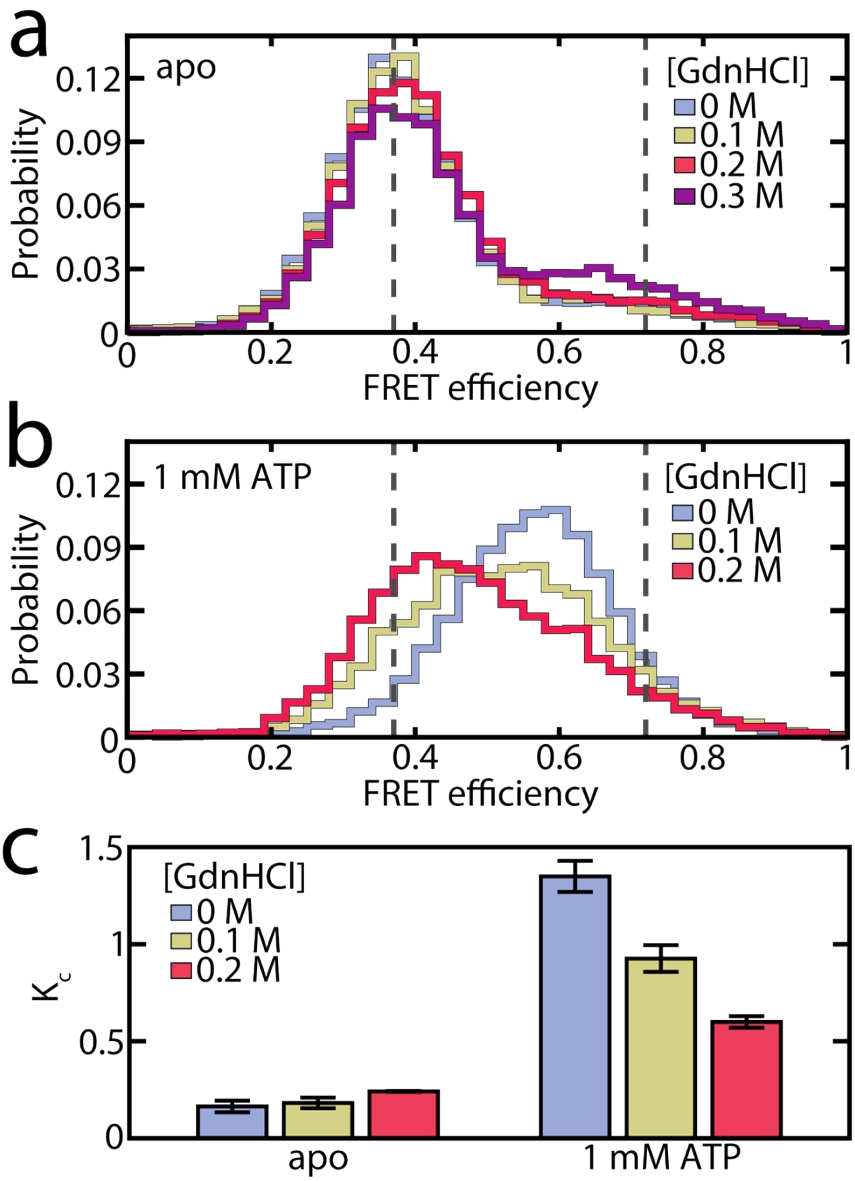

Figure S5: The effect of guanidine hydrochloride (GdnHCl) on the occupancy of the closed state. (a) FRET efficiency histograms of the apo AK at increasing GdnHCl concentrations. The dashed grey lines mark the FRET efficiency values of the open (0.37 ± 0.01) and closed (0.72 ± 0.01) states, as determined by H^{2}MM analysis. Up to 0.2 M GdnHCl (blue to red), the impact on the FRET efficiency histogram of the apoprotein is weak. At 0.3 M GdnHCl (violet), a more significant shift is observed, likely indicating the formation of a more compact folding intermediate,[19, 20] consistent with effects seen using urea (Fig. S3). (b) FRET efficiency histograms in the presence of 1 mM ATP. The addition of GdnHCl shifts the histogram towards lower FRET efficiencies, suggesting a redistribution of conformational states. c) The conformational equilibrium constant K_C (ratio of closed to open states) at 0 M (blue), 0.1 M (yellow), and 0.2 M (red) GdnHCl, shown both for the apoprotein (left) and in the presence of 1 mM ATP (right). Error bars represent the standard error of the mean of at least three independent measurements. GdnHCl affects the equilibrium distribution between open and closed states in a manner similar to urea but at lower concentrations, in agreement with the findings of Zhang *et al.* with respect to enzymatic activity.[21]

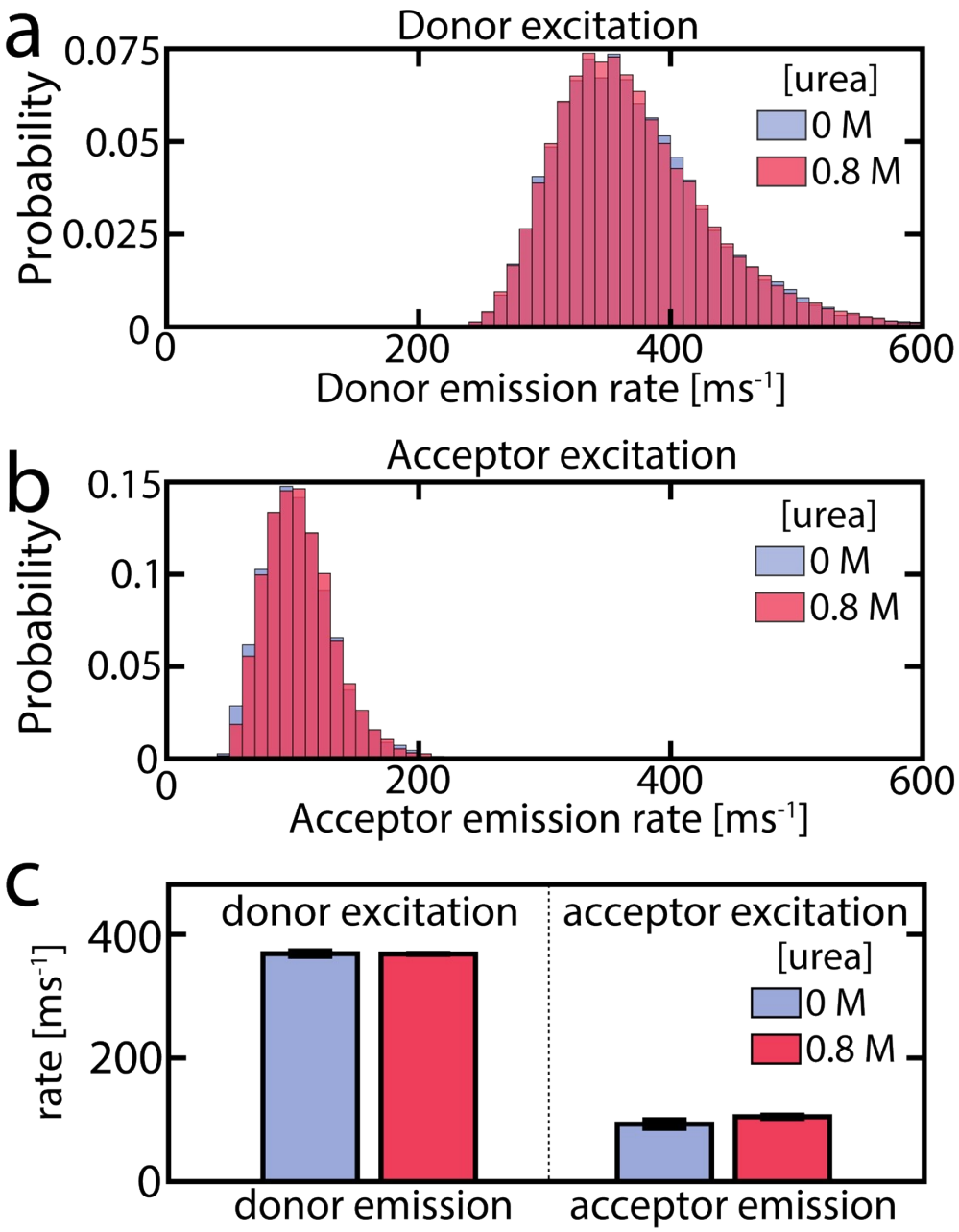

Figure S6: Urea does not affect the photon emission rates of the fluorescently labeled protein. a) Histogram of photon emission rates of individual AK molecules labeled with the donor dye (Alexa488) in the absence (blue) and presence (red) of urea after donor excitation. b) Same for the acceptor dye (Alexa594) after acceptor excitation. The laser power for acceptor excitation (10 μW) was lower than for donor excitation (50 μW), matching measurements of the double-labeled protein. c) Average photon emission rates from four independent measurements. The left panel shows donor emission after donor excitation, and the right panel shows acceptor emission after acceptor excitation. Error bars represent the standard error of the mean of at least three independent measurements. No significant differences were observed between measurements without (blue) and with (red) urea, indicating that urea did not affect the brightness of the fluorescent dyes in any significant manner.

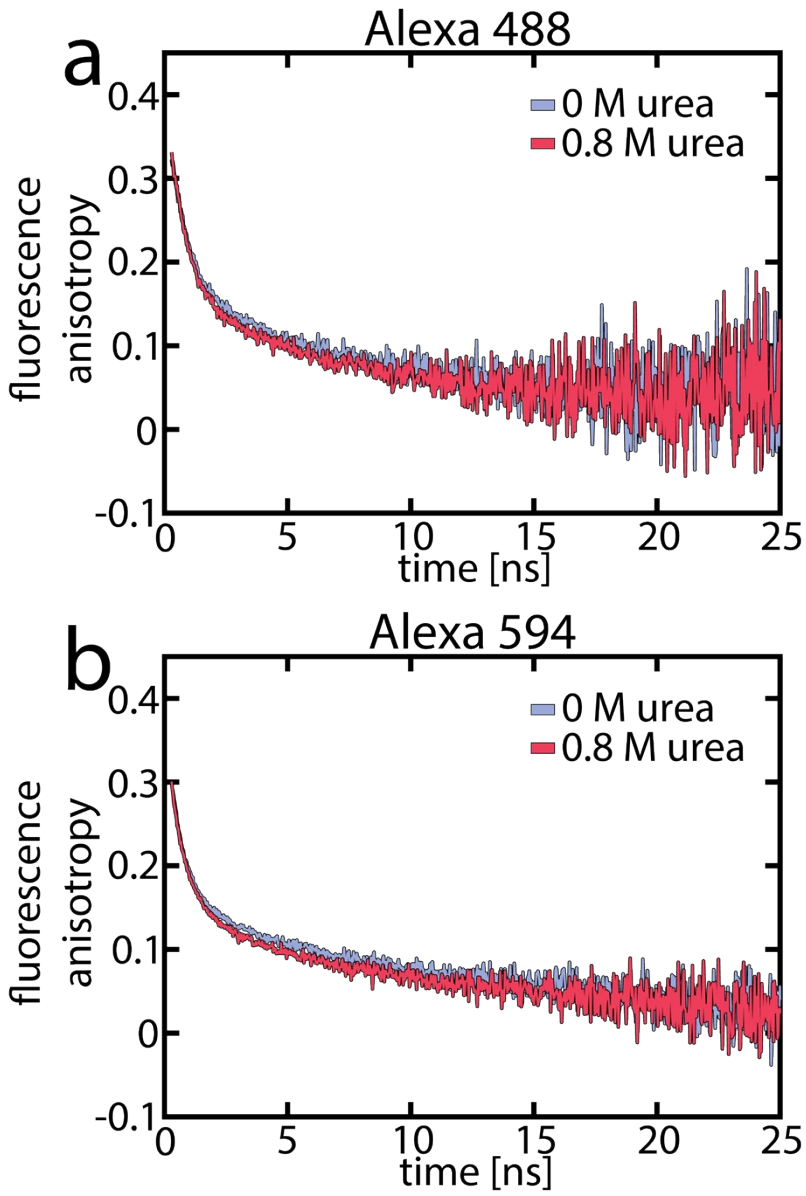

Figure S7: No effect of urea on dye mobility. a) Time-resolved fluorescence anisotropy measurements of apo AK labeled with Alexa488 (a) or Alexa 594 (b). The anisotropy decays were calculated according to Eq. (6) and are shown in the absence (blue) and presence of 0.8 M urea (red). The fast decay component indicates that the dyes at the labeling positions were not significantly constrained, while the slower decay was attributed to the rotational motion of the protein. No effect of urea on the rotational motion of the dyes was observed.

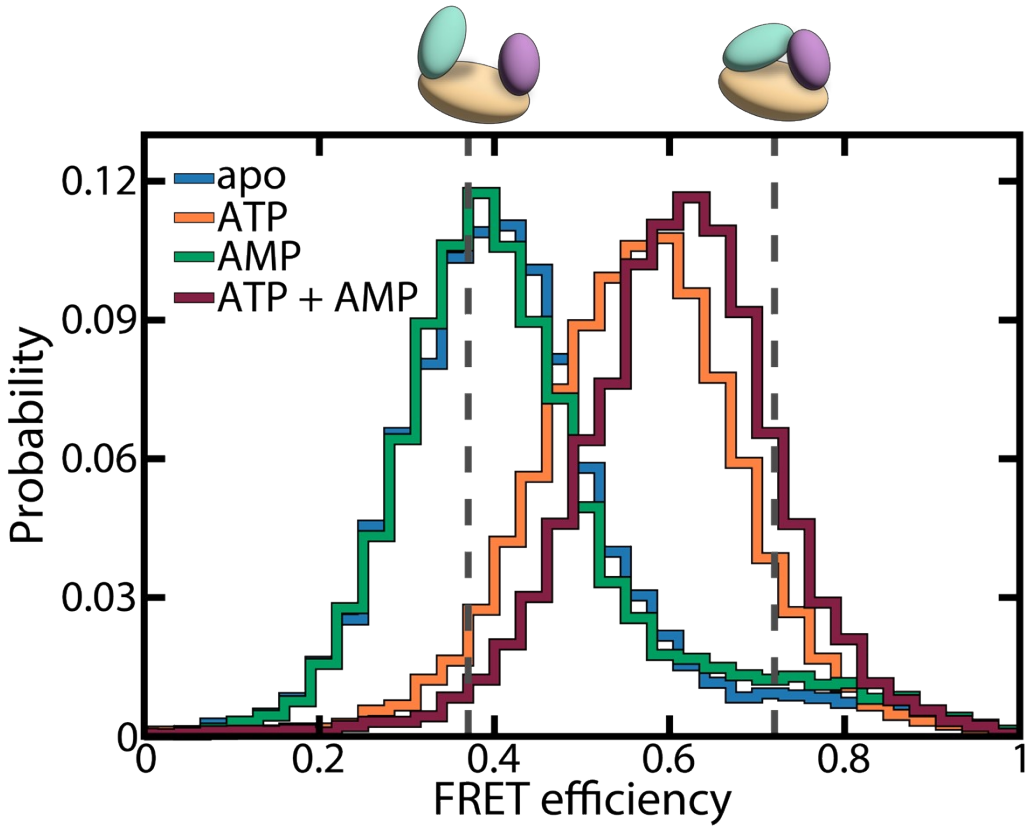

Figure S8: Substrate-dependent domain closure. The apoprotein (blue trace) mainly adopted an open conformation, occasionally exploring the closed state. AMP as a single substrate (5 mM, green) did not trigger significant closure of the LID domain. The binding of ATP (1 mM, orange) increased the population of the closed state. The additional presence of AMP (5 mM, red) shifted the histogram even more towards higher FRET efficiencies. The dashed grey lines indicate the FRET efficiencies of the open (0.37±0.01) and closed (0.72±0.01) state according to H^{2}MM analysis.[1]

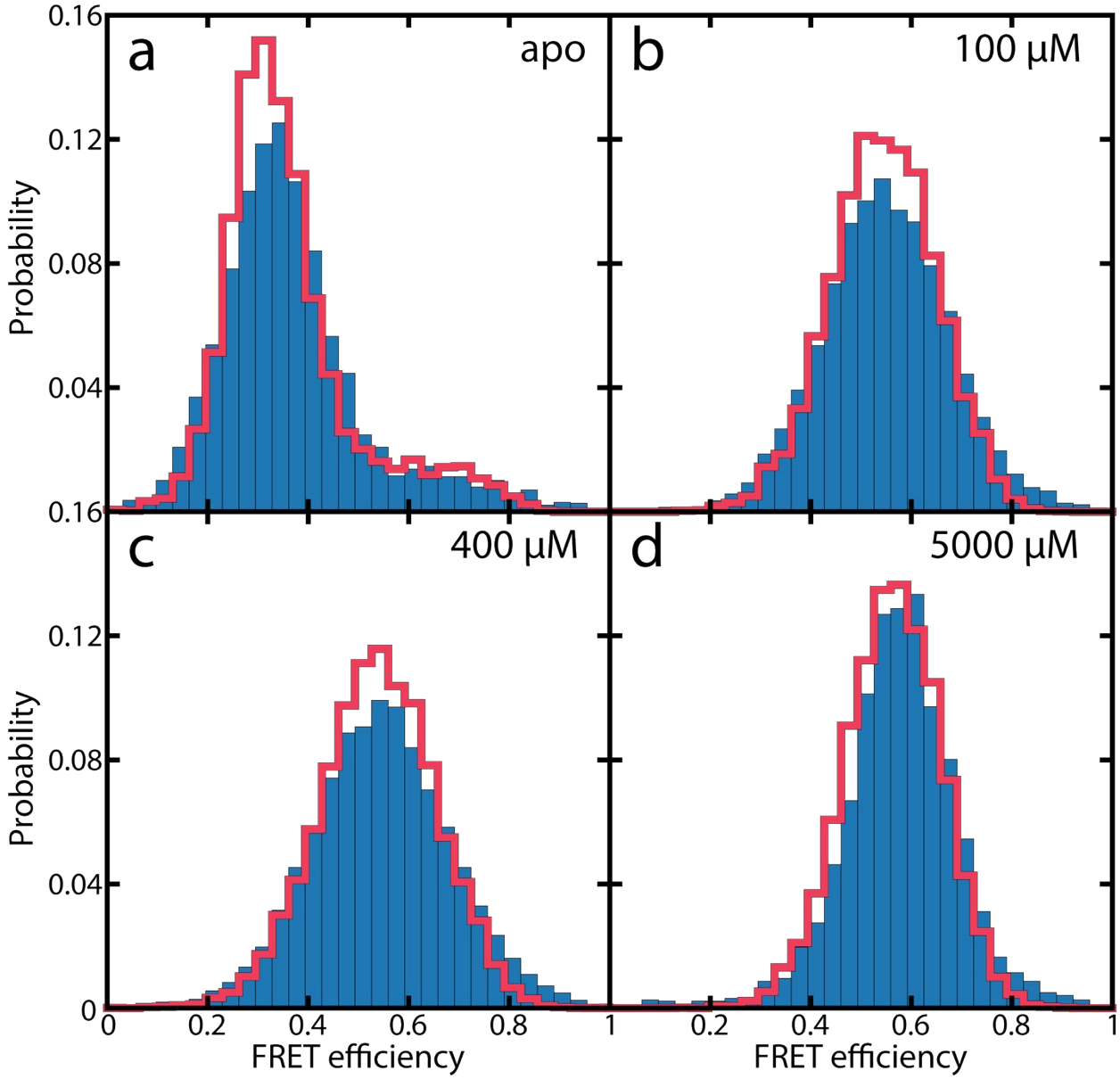

Figure S9: Validating H²MM models using recoloring. Representative experimental histograms are shown in blue for different AMP concentrations, as indicated in each panel. The recolored histograms are depicted as solid red lines and show good agreement between simulation and experiment. In b-d), the ATP concentration was fixed at 1 mM, and the ADP concentration was adjusted to guarantee equilibrium (Table S4).

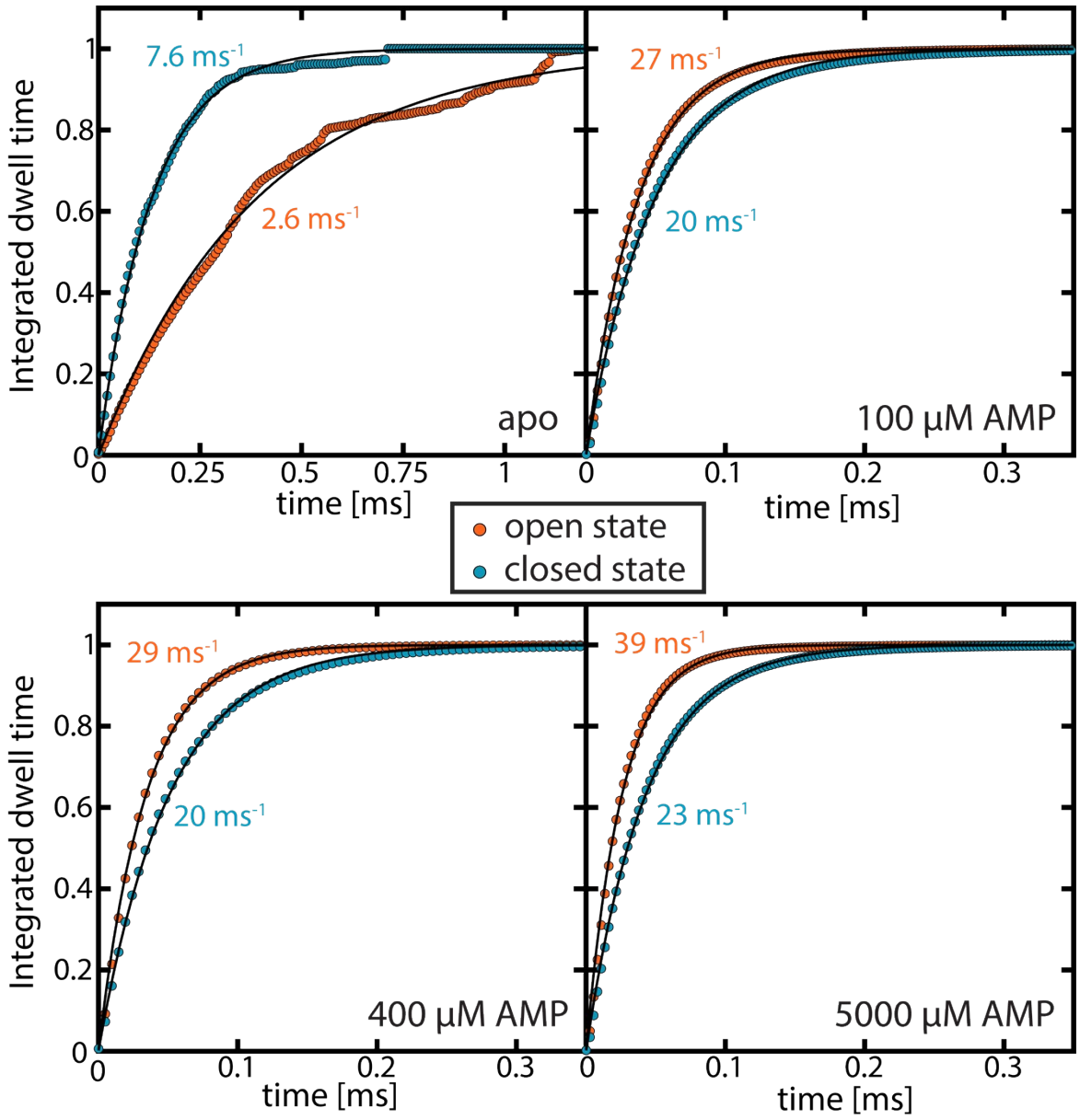

Figure S10: Dwell-time analysis. Integrated dwell-time distributions are shown for the open state (orange) and the closed state (cyan) at four different concentrations of AMP, as indicated within each panel. In b-d), the ATP concentration was fixed at 1 mM, with the ADP concentration adjusted to maintain equilibrium. Black lines represent fits to single-exponential functions. Both closing and opening rates extracted from the dwell time distributions compare favorably to the rates obtained by H^2MM analysis (Table S3).

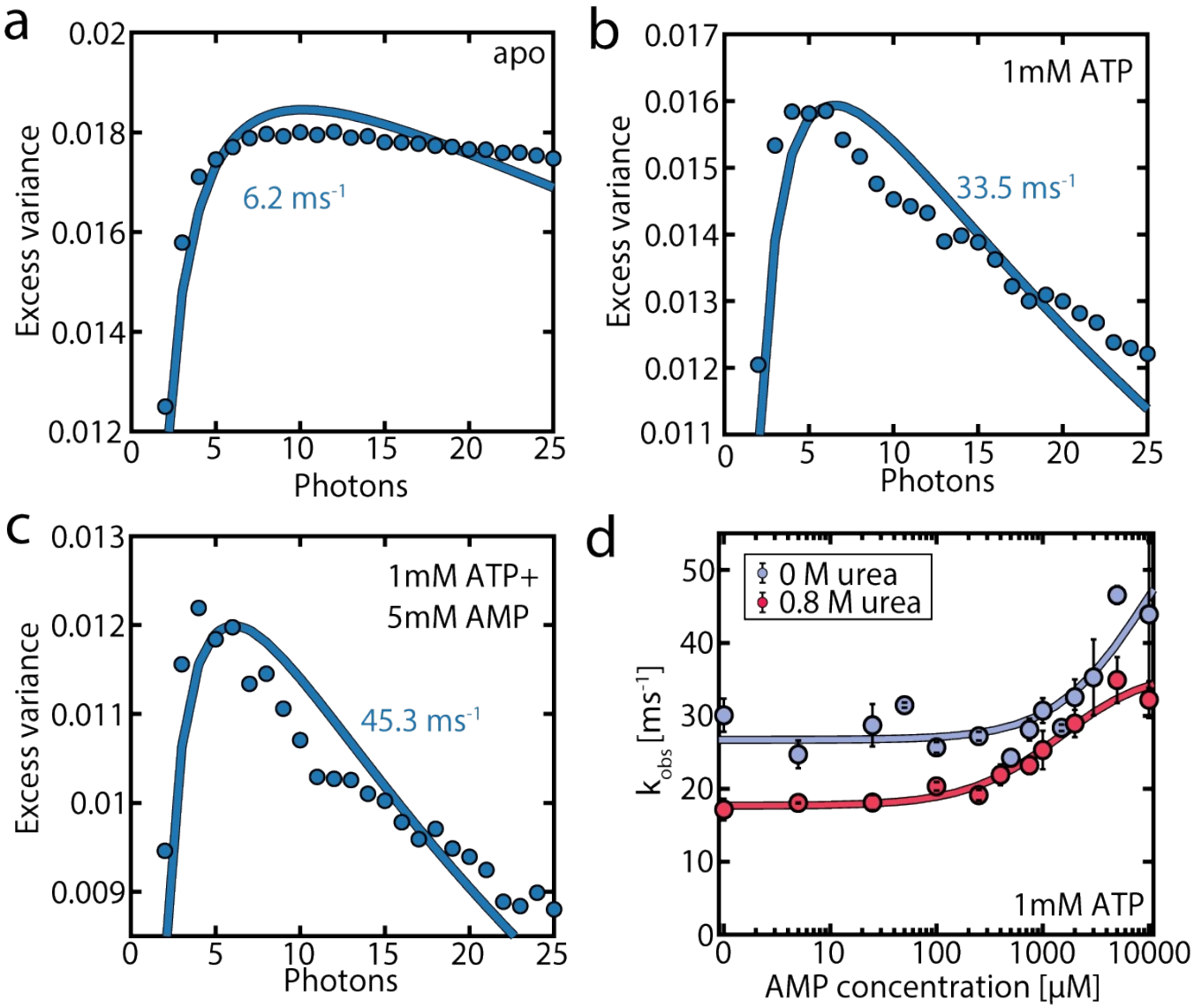

Figure S11: Time-resolved burst variance analysis (trBVA**)**. a-c) Traces of the excess variance with increasing numbers in the photon segments.[10] Solid lines represent fits to a model with 2 conformational states. The fits have two fitting parameters, the amplitude $<\delta\varepsilon^2>$ and the observed rate $k_{obs} = k_o + k_c$. trBVA confirms the presence of protein dynamics on the µs-time scale, which are accelerated by adding substrates. d) The observed rate k_{obs} as a function of AMP concentration for a fixed concentration of ATP (1 mM). The data set used is the same data set used to generate Fig. 4 in the main text, error bars indicate the standard error of the mean of at least 3 measurements. The solid lines indicate a fit to a binding isotherm. In agreement with H^{2}MM analysis, in the absence of AMP, k_{obs} is slowed down in the presence of urea (red curve). Likewise, the rates are accelerated by adding AMP, both in the presence and absence of urea. The observed rates reported in (d) are ~2 times slower than the sum $k_o + k_c$ in the H^{2}MM results (Fig. 4), a result that lies within the expected deviation from the ground truth for trBVA.[10]

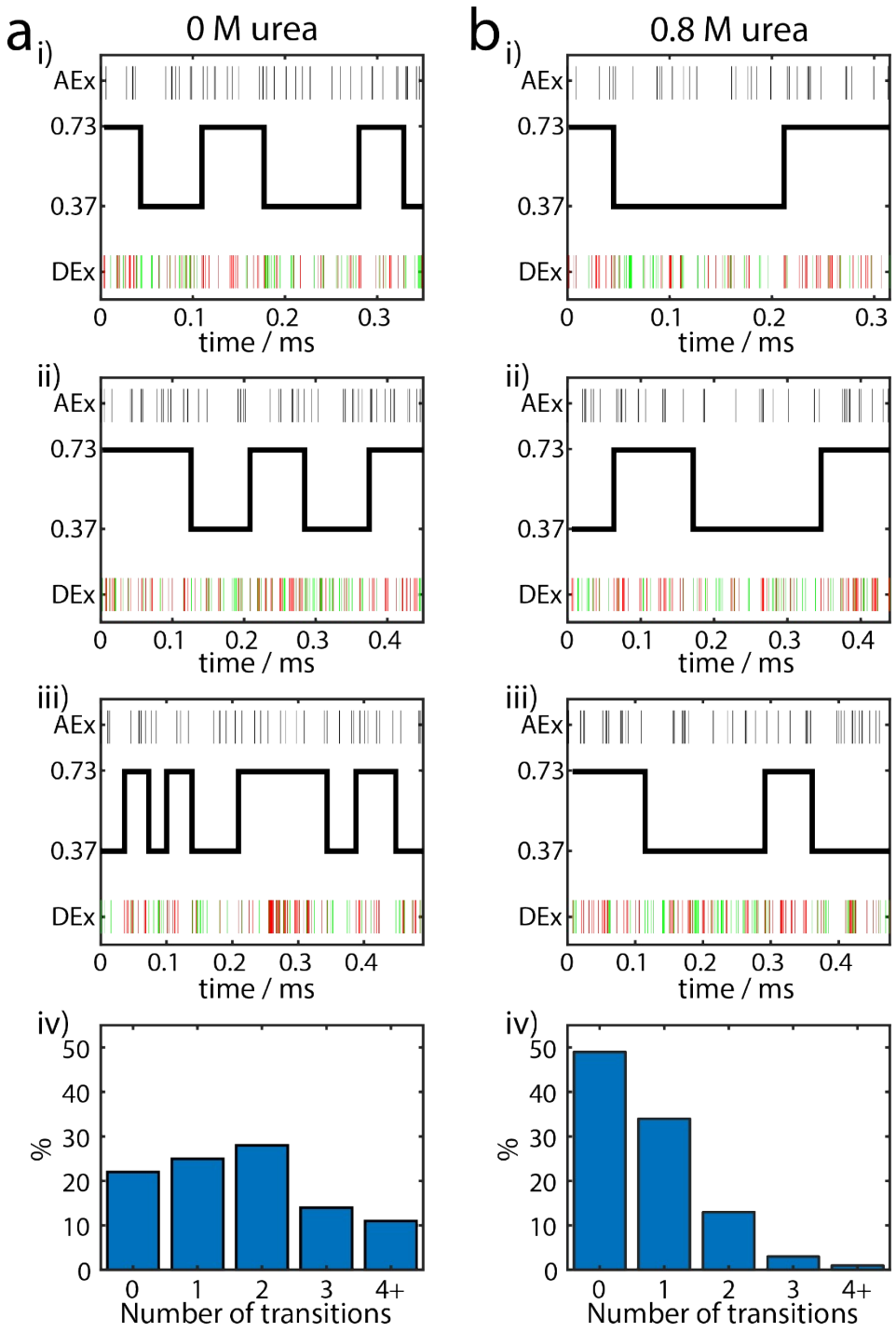

Figure S12: Representative photon-by-photon trajectories and Viterbi assignments. Single-molecule trajectories are shown for the WT protein at 1 mM ATP in (a) the absence of urea and (b) the presence of 0.8 M urea. For i-iii), the top panel shows the arrival time of photons after the acceptor pulse. The bottom panel shows the arrival time of photons after the donor pulse, in green for donor photons and red for acceptor photons. The black solid line depicts the most likely state sequence according to a Viterbi assignment.[8] iv) depicts the distribution of the number of transitions identified by the Viterbi algorithm in each data set. In the presence of only ATP, urea slows down the transition rates (main text Fig. 4), leading to fewer transitions in (b).

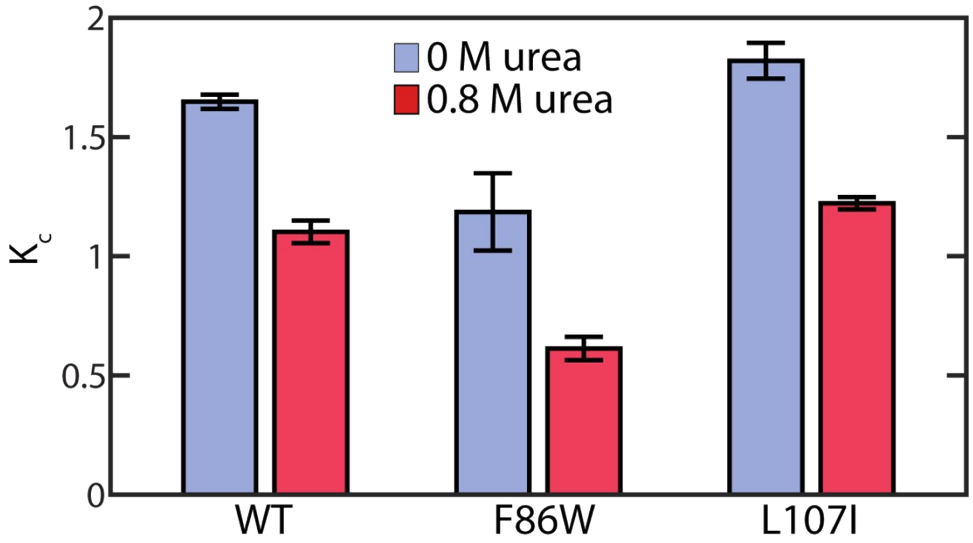

Figure S13: The effect of urea on the occupancy of the closed state for the mutant proteins. a) The equilibrium coefficient K_C for the mutant proteins F86W and L107I at with 1 mM ATP, 5 mM AMP and 417 μM ADP. The non-inhibited F86W and the strongly inhibited L107I are both shifted towards the open state by urea. Also, L107I has a slightly higher occupancy of the closed state than the WT, while for F86W K_C is lower. Error bars indicate the standard error of the mean of at least 3 measurements.

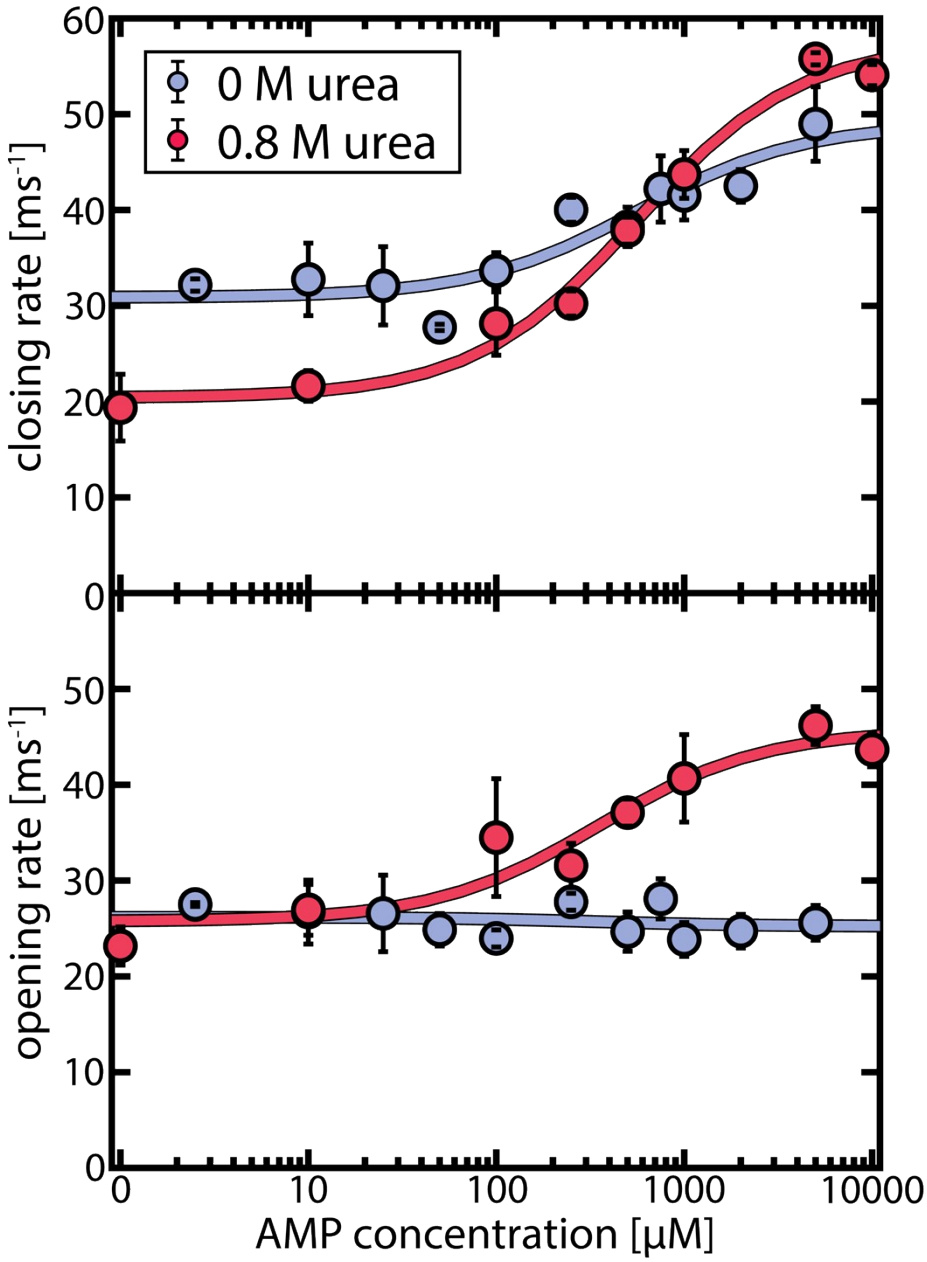

Figure S14: AMP-dependent closing and opening rates for L107I. Closing (upper panel) and opening (lower panel) rates for the L107I protein as a function of AMP concentration. Experiments were conducted at a fixed ATP concentration of 1 mM. Blue corresponds to the absence of urea, and red to the presence of 0.8 M urea. Solid lines indicate fits to a model described in "Supporting Note 2: Analysis of binding-state dependent opening and closing rates". The error bars indicate the standard error of the mean of 3 measurements.

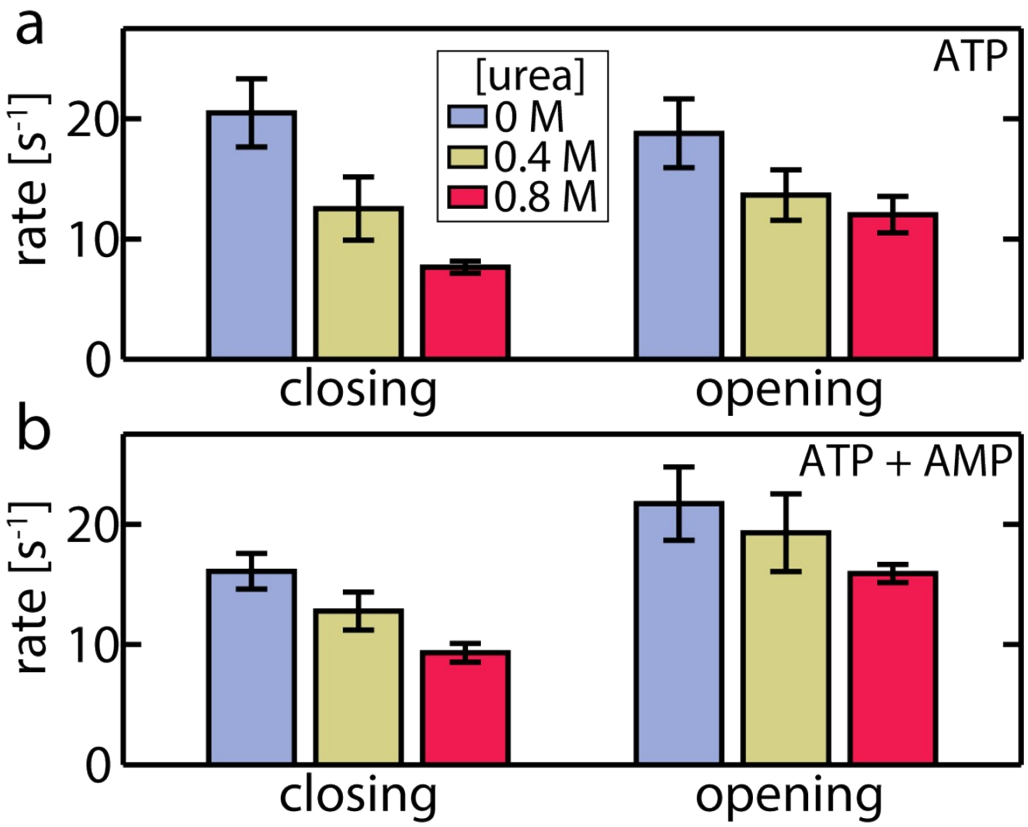

Figure S15: Effect of urea on the closing and opening rates of F86W. Closing (upper panel) and opening (lower panel) rates for the F86W protein as a function of the urea concentration, for a) 1000 μM ATP and b) 1000 μM ATP, 5000 μM AMP and 417 μM ADP. The error bars indicate the standard error of the mean of 3 measurements. Blue corresponds to the absence of urea, yellow to 0.4 M urea, and red to 0.8 M urea. For F86W, urea had a more pronounced impact on domain closing than opening, similar to both the WT (Fig. 4, main text) and L107I (Fig. S14) in the absence of inhibiting concentrations of AMP. Furthermore, comparing the values between (a) and (b) indicated that the addition of AMP to the ATP-bound protein did not cause statistically significant changes ($P > 0.05$, Student's t-test), unlike in the other proteins in the presence of high concentrations of AMP (Fig. 4 main text, Fig. S14).[1] This suggested that the "AMP first" pathway is only very weakly populated or not at all in F86W.

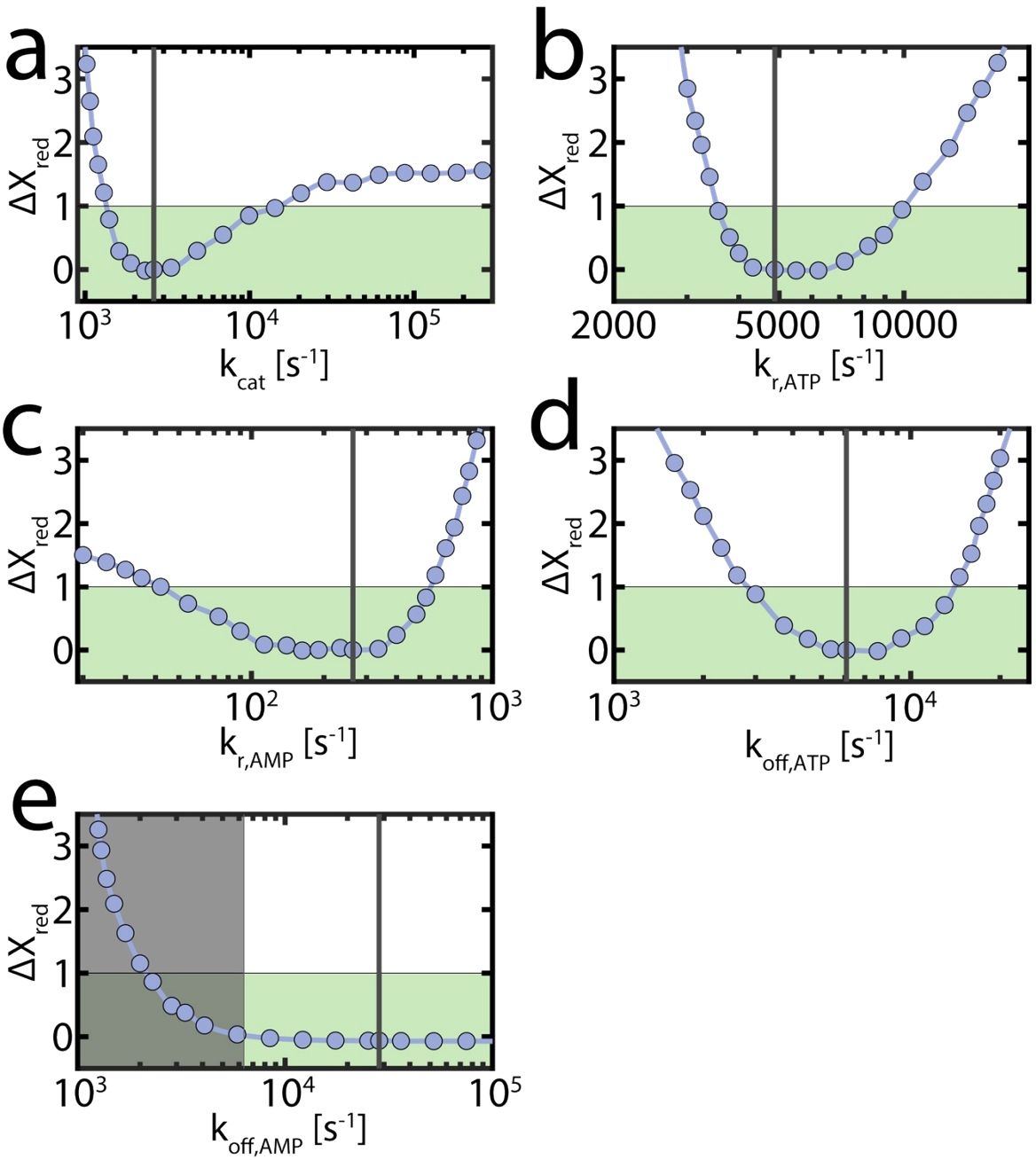

Figure S16: Confidence limits of parameters describing the enzymatic activity of WT AK. To estimate the parameters describing the enzymatic activity of AK, we used a χ^2-minimization. These parameters are a) k_{cat}, b) $k_{r,ATP}$ and c) $k_{r,AMP}$. We additionally fitted in (d) and (e) the explicit values for the dissociation rates $k_{off,ATP}$ and $k_{off,AMP}$, with a lower limit taken from NMR experiments[15, 16] indicated by the grey box in (e). Nucleotide binding rates were derived from the dissociation rates together with the measured K_d values. To estimate the confidence intervals of the fitted parameters, we monitored the increase in χ^2 per degree of freedom, χ^2_{red}, upon the perturbation of each parameter. For this, we used the optimized values from the χ^2 minimization (indicated by the black lines) and fixed the tested parameter at different values surrounding the optimal one. Then, the remaining parameters were optimized under this constraint, and we calculated the difference in χ^2_{red} with and without the constraint, $\Delta\chi^2_{red}$, indicated by

the blue dots. A $\Delta\chi^2_{red}$ value of 1 represents a 68.3 % confidence interval.[23] For example, a sharp increase in $\Delta\chi^2_{red}$ was observed when k_{cat} dropped below $1.5 \cdot 10^3$ s^{-1} (panel a). In contrast, the upper limit was less reliable, as a fast catalysis could be compensated to some extent by other parameters, in particular a faster rate for $k_{off,AMP}$. Notably, this analysis did not take into account physical reasonableness of the parameters; a very high rate for $k_{off,AMP}$ means that $k_{on,AMP}$ would exceed the diffusion limit in order to maintain experimental K_d values, which is unlikely.

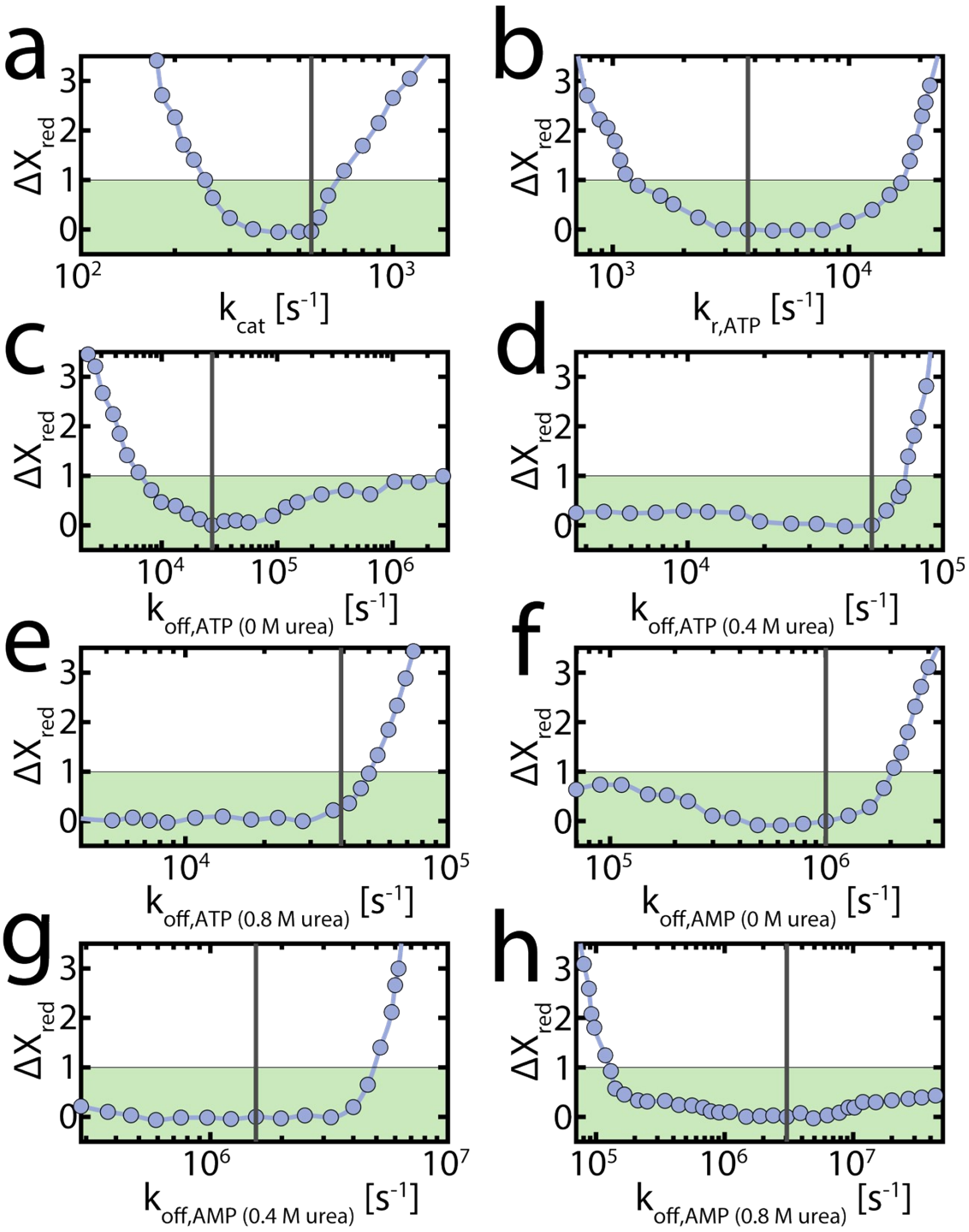

Figure S17: Confidence limits for the enzymatic parameters of the non-inhibited mutant F86W. As in Fig. S16, the change in χ^2_{red} upon perturbation of the optimal values (black lines) was monitored. These parameters are a) k_{cat}, b) $k_{r,\ ATP}$, c-e) $k_{off,\ ATP}$ and f-h) $k_{off,\ AMP}$. In contrast to Fig. S16, the dissociation rates were fitted without applying a restriction on K_d, to accommodate for potential changes in nucleotide affinity introduced by the mutation. F86 is located close to the AMP-binding site, causing a large increase in $k_{off,\ AMP}$, in agreement with results of Liang *et al.*.[18] For the non-inhibited F86W, the enzymatic velocity could be fitted with a simplified model containing only the "ATP first" pathway. A $\Delta\chi^2_{red}$ value of 1 represents a 68.3 % confidence interval, which is indicated by the green box.

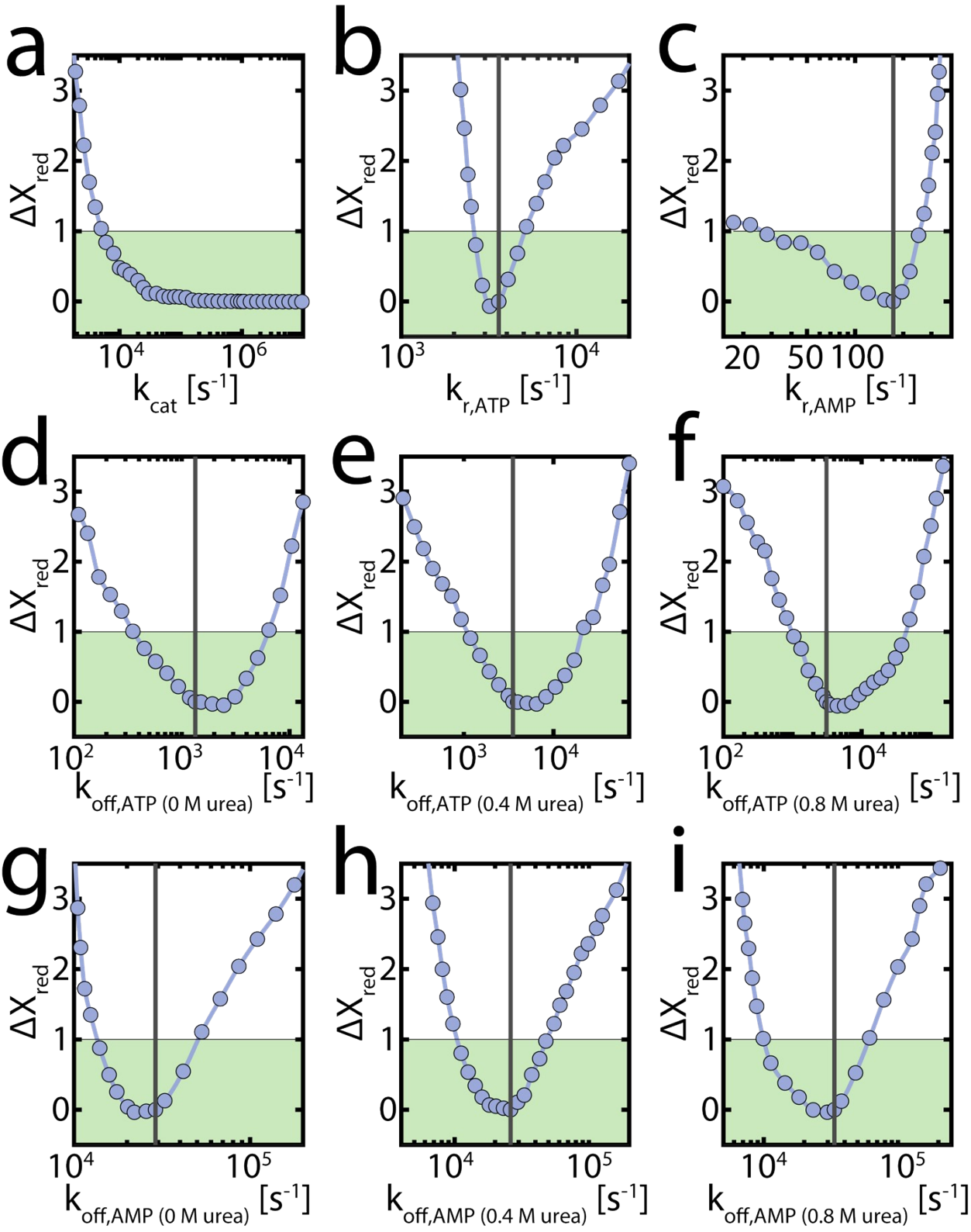

Figure S18: Confidence limits for the enzymatic parameters of the strongly inhibited mutant L107I. As in Fig. S16, the change in χ^2_{red} upon perturbation of the optimal values (black lines) was monitored. These parameters are a) k_{cat}, b) $k_{r,ATP}$, c) $k_{r,AMP}$, d-f) $k_{off,ATP}$ and g-i) $k_{off,AMP}$. The dissociation rates were fitted without applying a restriction

on K_d, to accommodate potential changes in nucleotide affinity introduced by the mutation. A $\Delta\chi^2_{red}$ value of 1 represents a 68.3 % confidence interval and is indicated by the green box.

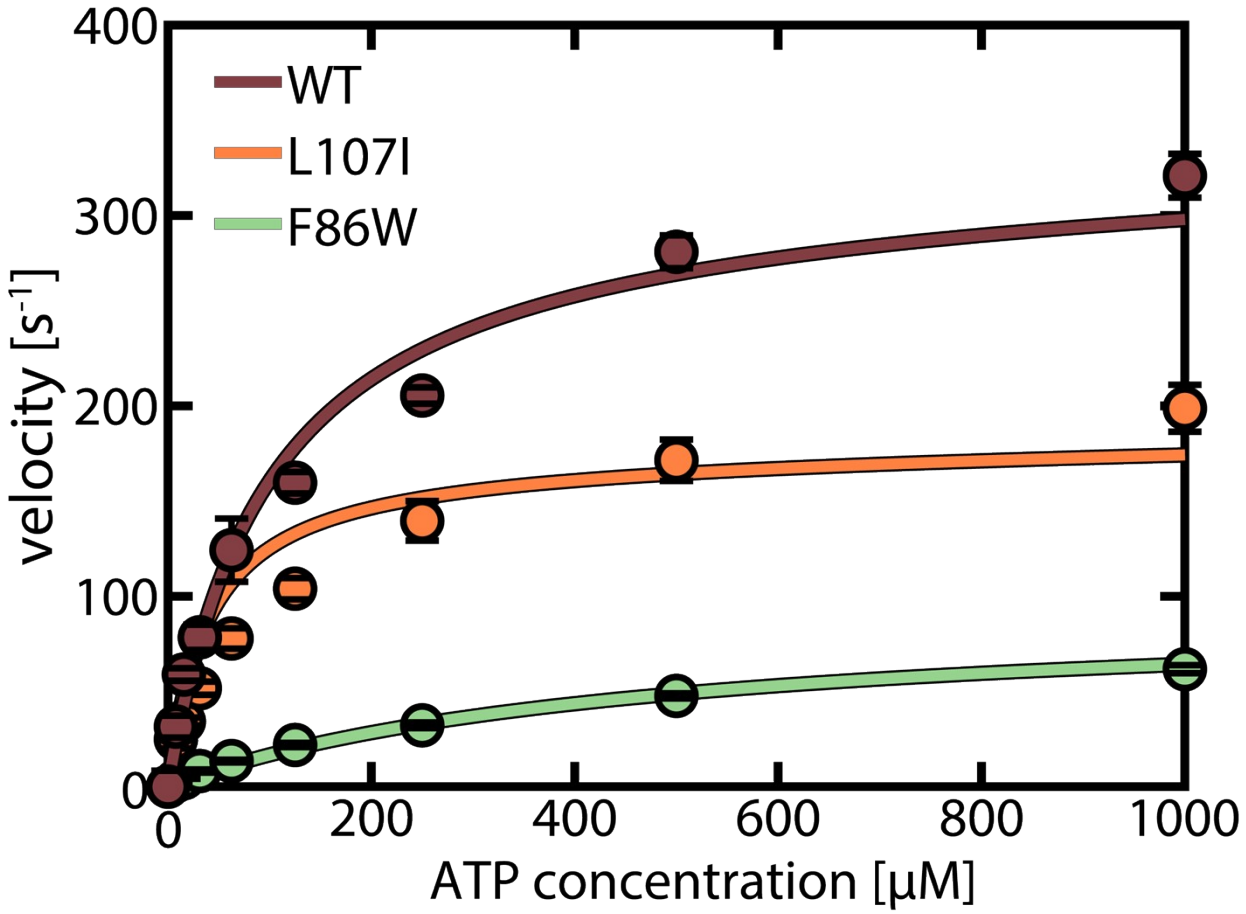

Figure S19. ATP-dependent activity for AK mutants. Enzymatic velocity as a function of ATP concentration for a fixed concentration of 1000 µM AMP and in the absence of urea. Shown are the WT protein (brown), L107I (orange) and F86W (green). The straight lines represent fits to the model described in "Supporting Note 1: Model for the substrate inhibition by AMP". The fit parameters are shared with the AMP-dependent activity (Fig. 1a-c main text) and given in Table 1 (main text).

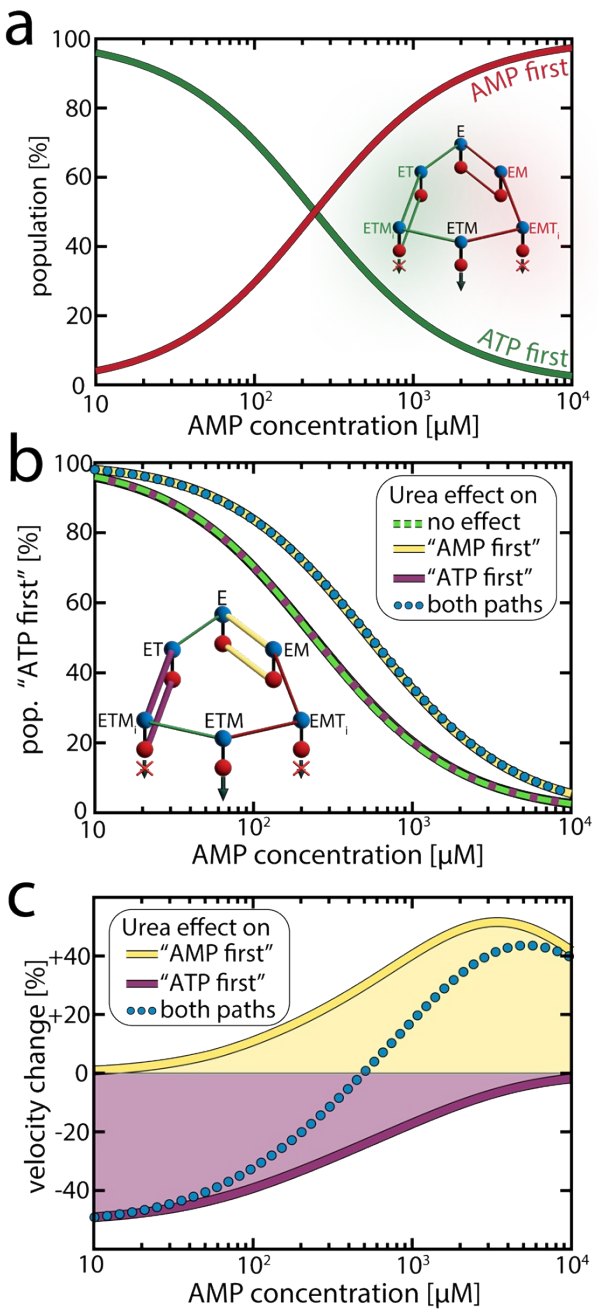

Figure S20. Population of the competing "ATP first" and "AMP first" pathways. To understand how the urea-induced reduction in AMP affinity can increase velocity, it is helpful to understand how the enzyme population is distributed between the two pathways.

a) The population of the two pathways as a function of the AMP concentration at 0 M urea, simulated according to our model for a fixed ATP concentration of 1 mM. The "ATP first" path in green contains the ET and ETM_i states and is dominating when the AMP concentration is small. The "AMP first" path in red contains the EM and EMT_i states and is becoming more populated as the AMP concentration increases. Both pathways are equally populated at 300-400 μM AMP, where the highest enzymatic velocity was observed (main text Fig. 1a). Further increasing the AMP concentration reduces the overall velocity, as the productivity loss in the "ATP first" path is more significant than the gain in the "AMP first" path due to the low k_r^{M-path}.

b) Change in the population of the "ATP first" path due to presence of urea. As in (a), we simulated the distribution of populations between the pathways. The dashed green curve depicts the population of the “ATP first” path in the absence of urea. To obtain the dotted blue line, we altered AMP affinity according to experimental observations, while preserving all other parameters, including those describing conformational dynamics, as determined at 0 M urea. The violet and yellow lines illustrate the impact on the population of the “ATP first” path when urea affects AMP affinity in only one of the two pathways. Although AMP binding is required in both pathways, decreasing its affinity had distinct effects in the two pathways. Increasing K_d (AMP) in the first step of "AMP first" path (highlighted in yellow in the inset) while preserving K_d (AMP) in the opposing path increased the likelihood of reaching the more productive "ATP first" path. In contrast, reducing the AMP affinity in the second step of the more productive "ATP first" path (highlighted in violet in the inset) hardly affected the distribution between the pathways.

c) Outcome of the urea-induced changes in the distribution between the pathways on enzymatic velocity. As shown in (b), reducing AMP affinity affected the distribution between the pathways differently depending on which pathway is affected. We simulated how these changes affect the overall enzymatic velocity. The yellow curve depicts the velocity change when urea affected only the affinity within the "AMP first" path (yellow), with AMP affinity in the opposing "ATP first" path preserved. The outcome at low AMP concentrations was negligible, as the "AMP first" path was scarcely populated. However, at intermediate concentrations, the overall velocity increased due to a higher population of the "ATP first" pathway (b). At very high AMP concentrations, the impact of urea was weak, as AMP binding was much faster than dissociation. In contrast, reducing AMP affinity within the "ATP first" path (violet) had a purely detrimental effect on velocity, as it reduced the flux through the productive pathway. The effect was strongest at low AMP levels, where this pathway was most populated, and lost significance as the "AMP first" path was more populated. The dotted blue line shows the velocity change when the affinity is reduced in both pathways.

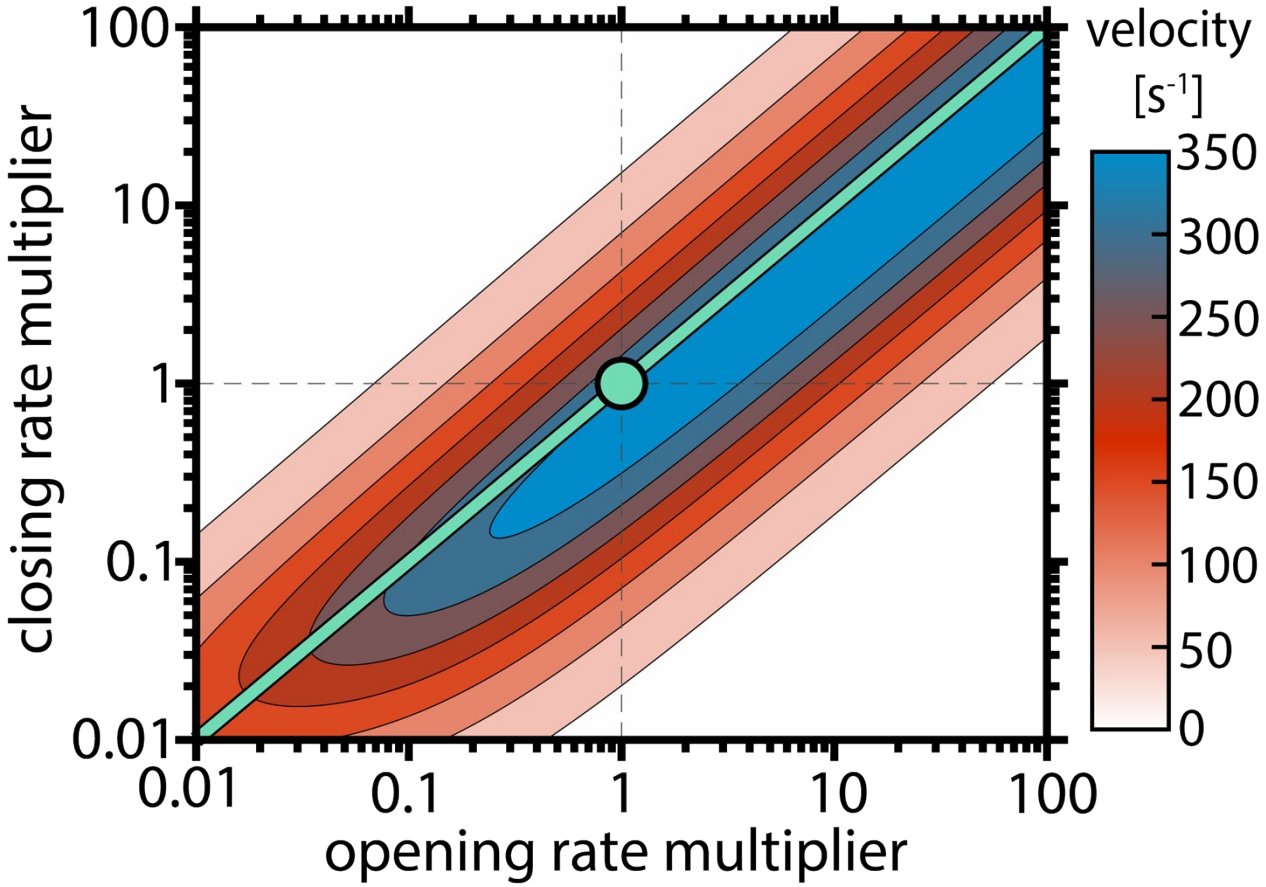

Figure 21. Enzymatic velocity as a function of the opening and closing rate at physiological concentrations of nucleotides. We simulated how the velocity changes when open and closing rates of the ATP-bound species (ET, ETM_i, EMT_i, ETM) are altered. The experimentally derived k_o and k_c were scaled by a factor between 0.01 and 100. Substrate concentrations of 0.3 mM AMP and 5 mM ATP reflected the physiological concentrations in *E.coli.*[24] The optimal open/closed ratio obtained in the calculation was close to the experimental K_C value (turquoise circle), suggesting the enzyme has evolved to optimize both K_C and transition rates for maximal turnover under physiological substrate concentrations.

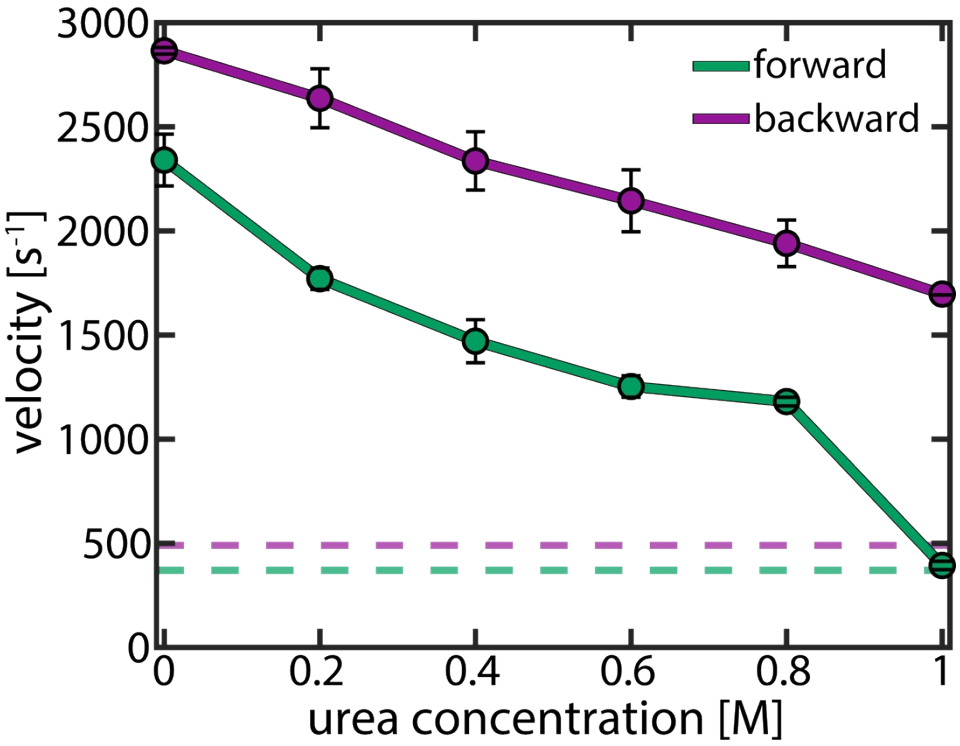

Figure S22: Activity of coupled enzymatic systems. A sufficient activity of the coupled enzymatic systems in the presence of urea must be guaranteed for a reliable assessment of AK's enzymatic velocity. The solid lines show the turnover of these systems for the forward (green) and backward (violet) reactions. Error bars represent the standard error of the mean of three measurements. For the forward reaction (MgATP + AMP → ADP + MgADP), AK's turnover was assessed using the system phosphokinase/ lactate dehydrogenase. We monitored the activity of this system in the absence of AK at different urea concentrations. The reaction was started by the injection of 2 mM ADP. Similarly, for the backward reaction (MgADP + ADP → AMP + MgATP), the relative turnover of the system hexokinase/ glucose-6-phosphate dehydrogenase was monitored after the addition of 2 mM ATP. In both cases, the addition of urea reduced turnover. However, the enzymatic velocity of the coupled system remained about three times faster than the maximum turnover of AK (dashed lines), except for 1 M urea (forward direction), where the velocity decreased strongly.

Table S1: Michaelis-Menten parameters for the backward reaction[a]

Urea concentration [M]	v_{max} [s^{-1}]	K_M [µM]
0	620(±17)	1340(±98)
0.2	578(±15)	1144(±83)
0.4	590(±27)	1064(±143)
0.6	621(±34)	1226(±184)
0.8	584(±27)	1030(±142)

[a] numbers in brackets indicate the standard error of the fit

Table S2: Change in non-linearity of steady-state time course due to alleviation of product inhibition [a]

ADP concentration [µM] [b]	η×10³		$\frac{\eta(0.8\ M\ urea)}{\eta(0\ M\ urea)}$
	η(0 M urea)	η(0.8 M urea)	
750	3.67(±1.17)	4.87(±1.28)	1.33 (±0.78)
1000	4.12(±1.41)	5.42(±2.22)	1.31(±0.97)
2000	6.21(±1.94)	4.85(±1.48)	0.78(±0.48)
3000	6.63(±1.54)	4.96(±1.02)	0.75(±0.33)
4000	6.87(±0.29)	5.17(±0.55)	0.75(±0.11)
5000	7.34(±0.60)	5.12(±0.24)	0.70(±0.09)

[a] number in brackets indicate the standard error of the mean from 3 measurements

[b] for low initial substrate concentrations (≤500 µM), where turnover numbers are small and little AMP is formed, a more reliable fit of turnover was obtained when η was set to 0.

Table S3: Comparison of transition rates obtained by H²MM vs. dwell-time analysis (DTA)[a]

AMP [µM]	Urea [M]	k_c [10^3 s^{-1}]		k_o [10^3 s^{-1}]	
		H²MM	DTA	H²MM	DTA
apo	0	1.0 (±0.2)	2.1 [b] (±0.5)	6.5 (±0.4)	5.2 (±1.7)
	0.2	0.7 (±0.2)	2.5 [b] (±0.7)	6.0 (±2.4)	6.2 (±0.7)
	0.4	0.9 (±0.1)	2.7 [b] (±0.4)	5.0 (±0.2)	6.8 (±2.3)
	0.6	0.8 (±0.1)	1.6 [b] (±0.1)	4.5 (±0.8)	4.5 (±1.2)
	0.8	0.8 (±0.1)	1.7 [b] (±0.6)	4.0 (±0.2)	4.7 (±0.5)
400	0	31.1 (±2.2)	29.9 (±2.9)	20.4 (±2.1)	18.6 (±2.2)
	0.2	27.1 (±1.7)	25.0 (±1.9)	22.1 (±1.0)	19.9 (±0.7)
	0.4	27.1 (±1.2)	25.0 (±1.5)	23.7 (±0.6)	21.5 (±0.7)
	0.6	25.6 (±3.9)	23.6 (±3.7)	22.9 (±2.9)	21.3 (±2.2)
	0.8	25.4 (±1.9)	22.9 (±1.5)	26.4 (±1.0)	24.0 (±0.4)
5000	0	46.6 (±0.4)	42.1 (±1.6)	28.3 (±0.9)	24.7 (±0.6)
	0.2	49.7 (±0.9)	47.5 (±1.7)	34.6 (±1.6)	29.9 (±1.6)
	0.4	44.9 (±1.9)	39.2 (±3.0)	33.9 (±2.2)	29.0 (±2.8)
	0.6	46.2 (±1.8)	40.6 (±0.8)	36.7 (±0.9)	31.5 (±2.0)
	0.8	40.1 (±4.1)	36.2 (±3.1)	36.2 (±2.4)	32.3 (±1.3)

[a] number in brackets indicate the standard error of the mean of at least three measurements

[b] dwell times extend the length of individual bursts (~250 µs given the chosen burst selection criteria), preventing a reliable analysis

Table S4: Substrate concentrations used in smFRET experiments

c_{ATP} fixed at 1 mM	
AMP [µM]	**ADP [µM]**
1	6.2
2.5	9.9
5	13.9
10	19.7
25	31
50	44
100	62
250	95
400	123
500	137
750	150
1000	160
2000	230
3000	327
5000	417
10000	576

Table S5: Protein dynamics parameters used in the fitting of enzymatic velocity

rate constants [ms^{-1}]		k_c			k_o		
		0 M urea	0.4 M urea	0.8 M urea	0M urea	0.4 M urea	0.8 M urea
WT	E	1.0	0.9	0.8	6.2	5.0	4.0
	EM	2.4	1.5	1.8	13	7.0	9.9
	ET / ETM / ETM$_i$ [a]	26	18	15	23	16	18
	EMT$_i$	49	45	43	23	34	37
F86W	E	0.35	0.20	0.22	3.7	1.8	1.4
	EM	0.37	0.27	0.21	3.4	3.1	1.4
	ET / ETM / ETM$_i$ [a,b]	20	13	7.7	19	14	12
	EMT$_i$ [b]	16	13	9.3	21	19	16
L107I	E	2.5	1.7	0.9	18	11	7.8
	EM	6.5	4.9	2.5	34	31	18
	ET / ETM / ETM$_i$ [a]	30	28	22	25	28	25
	EMT$_i$	57	55	55	32	45	45

[a] The single-molecule experiments cannot distinguish between ET, ETM and ETM$_i$.

[b] Differences between ET/ETM/ ETM$_i$ and EMT$_i$ in F86W are not statistically significant.

Table S6: Parameters for the unfolding of AK measured by CD spectroscopy

	ΔG^{0}_{fold} [kJ mol^{-1}]	m [kJ mol^{-1} M^{-1}]	midpoint [M]
without substrates	19.7	7.0	2.82
with substrates	28.9	9.0	3.19

Supporting References

1. D. Scheerer, B. V. Adkar, S. Bhattacharyya, D. Levy, M. Iljina, I. Riven, O. Dym, G. Haran and E. I. Shakhnovich, Allosteric communication between ligand binding domains modulates substrate inhibition in adenylate kinase, *Proceedings of the National Academy of Sciences*, 2023, **120**, e2219855120.
2. J. Lu, D. Scheerer, W. Wang, G. Haran and W. Li, Role of repeated conformational transitions in substrate binding of adenylate kinase, *The Journal of Physical Chemistry B*, 2022, **126**, 8188-9201.
3. G. Maglia, N. Galenkamp, S. Zernia, Y. Van Oppen and A. Milias-Argeitis, Allostery can convert binding free energies into concerted domain motions in enzymes, *Research Square*, 2024.
4. H. Y. Aviram, M. Pirchi, H. Mazal, Y. Barak, I. Riven and G. Haran, Direct observation of ultrafast large-scale dynamics of an enzyme under turnover conditions, *PNAS*, 2018, **115**, 3243-3248.
5. X. R. Sheng, X. Li and X. M. Pan, An iso-random Bi Bi mechanism for adenylate kinase, *Journal of Biological Chemistry*, 1999, **274**, 22238-22242.
6. S. Kuby and E. Noltman, ATP-Creatine Transphosphorylase. The Enzymes.*Journal*, 1962.
7. I. V. Gopich and A. Szabo, Decoding the pattern of photon colors in single-molecule FRET, *The Journal of Physical Chemistry B*, 2009, **113**, 10965-10973.
8. M. Pirchi, R. Tsukanov, R. Khamis, T. E. Tomov, Y. Berger, D. C. Khara, H. Volkov, G. Haran and E. Nir, Photon-by-photon hidden Markov model analysis for microsecond single-molecule FRET kinetics, *J. Phys. Chem. B*, 2016, **120**, 13065-13075.
9. M. Pirchi, PhD, Weizmann Institute of Science, 2013.
10. I. Terterov, D. Nettels, D. E. Makarov and H. Hofmann, Time-resolved burst variance analysis (trBVA), *Biophysical Reports*, 2023, 100116.
11. C. N. Pace, in *Methods in Enzymology*, Academic Press, 1986, vol. 131, pp. 266-280.
12. O. Acevedo, M. Guzman-Casado, M. M. Garcia-Mira, B. Ibarra-Molero and J. M. Sanchez-Ruiz, pH Corrections in Chemical Denaturant Solutions, *Analytical Biochemistry*, 2002, **306**, 158-161.
13. P. Rogne and M. Wolf-Watz, Urea-Dependent Adenylate Kinase Activation following Redistribution of Structural States, *Biophysical Journal*, 2016, **111**, 1385-1395.
14. C. Tanford, Isothermal Unfolding of Globular Proteins in Aqueous Urea Solutions, *Journal of the American Chemical Society*, 1964, **86**, 2050-2059.
15. D. C. Fry, S. A. Kuby and A. S. Mildvan, NMR studies of the magnesium-ATP binding site of adenylate kinase and of a 45-residue peptide fragment of the enzyme, *Biochemistry*, 1985, **24**, 4680-4694.
16. D. C. Fry, S. A. Kuby and A. S. Mildvan, NMR studies of the AMP-binding site and mechanism of adenylate kinase, *Biochemistry*, 1987, **26**, 1645-1655.
17. MATLAB, 9.14.0.2206163 (R2023a), 2023.
18. P. Liang, G. N. Phillips Jr. and M. Glaser, Assignment of the nucleotide binding sites and the mechanism of substrate inhibition of Escherichia coli adenylate kinase, *Proteins: Structure, Function, and Bioinformatics*, 1991, **9**, 28-36.
19. H. Mazal, H. Aviram, I. Riven and G. Haran, Effect of ligand binding on a protein with a complex folding landscape, *Physical Chemistry Chemical Physics*, 2018, **20**, 3054-3062.
20. T. P. Schrank, D. W. Bolen and V. J. Hilser, Rational modulation of conformational fluctuations in adenylate kinase reveals a local unfolding mechanism for allostery and functional adaptation in proteins, *Proceedings of the National Academy of Sciences*, 2009, **106**, 16984-16989.
21. H.-J. Zhang, X.-R. Sheng, X.-M. Pan and J.-M. Zhou, Activation of Adenylate Kinase by Denaturants Is Due to the Increasing Conformational Flexibility at Its Active Sites, *Biochem. Biophys. Res.*, 1997, **238**, 382-386.

22. H. Rastogi, A. Singh and P. K. Chowdhury, Towards the energy landscape of adenylate kinase in crowded milieu: Activity, conformation, structure and dynamics in sequence, *Archives of Biochemistry and Biophysics*, 2023, 109658.
23. W. T. Vetterling, *Numerical recipes example book (c++): The art of scientific computing*, Cambridge University Press, 2002.
24. O. H. Lowry, J. Carter, J. B. Ward and L. Glaser, The Effect of Carbon and Nitrogen Sources on the Level of Metabolic Intermediates in Escherichia coli, *Journal of Biological Chemistry*, 1971, **246**, 6511-6521.